Geerts, B., T. Andretta, S. Luberda, J. Vogt, Y. Wang, and L. D. Oolman, 2009: A case study of a long-lived tornadic mesocyclone in a low-CAPE complex-terrain environment. *Electronic J. Severe Storms Meteor.*, **4** (3), 1-29.

Electronic Journal of
SEVERE STORMS METEOROLOGY

A Case Study of a Long-lived Tornadic Mesocyclone in a Low-CAPE Complex-terrain Environment

B. GEERTS, T. ANDRETTA, S. J. LUBERDA, J. VOGT, Y. WANG, AND L. D. OOLMAN
Department of Atmospheric Science, University of Wyoming

JONATHAN FINCH
NOAA / NWS, Weather Forecast Office, Dodge City, Kansas

DAN BIKOS
Cooperative Institute for Research in the Atmosphere, Colorado State University, Fort Collins, Colorado

(Submitted 18 May 2009; in final form 30 December 2009)

ABSTRACT

On 22 May 2008 a long-lived mesocyclone spawned an EF2 tornado over terrain as high as 2650 m MSL in southeastern Wyoming. The mesocyclone was part of an elongated, complex storm system that grew rather early in the day near a slow-moving warm front. The mesocyclone is unusual in that it persisted and became tornadic in rather cold (~7°C), saturated surface conditions in an environment with CAPE < 1000 J kg^{-1} and no surface-based convective inhibition. The mesocyclone intensified as its parent storm moved over terrain gradually ascending by ~1000 m, reaching a radar-estimated low-level horizontal shear as high as 84 m s^{-1} km^{-1}. This fast-moving mesocyclone could be tracked by the nearest Doppler radar for over 90 min.

This paper examines the characteristics and the environment of this mesocyclone using both operational weather data and high-resolution numerical simulations. Near-surface radar observations and model output suggest that the formation and maintenance of the mesocyclone in this low-CAPE environment benefited from two terrain-related factors. One is the observed channeling of the low-level flow, locally enhancing the storm-relative helicity. The second is the presence, suggested by high-resolution simulations, of banners of high potential vorticity generated by the strong southerly flow shearing around the Colorado Front Range.

1. Introduction

Tornadogenesis is a major forecast challenge in regions of complex terrain (e.g., Homar et al. 2003). For instance, low-level storm-relative helicity (SRH), known to affect tornado potential, can vary dramatically over short distances due to topographically-channeled flow (e.g., Braun and Monteverdi 1991; Bosart et al. 2006). Tornadoes are relatively uncommon in the arid high-plain and mountain environment of Wyoming (Brooks et al. 2003a), although they may be underreported because of the low population density (Anderson et al. 2007).

Corresponding author address: Bart Geerts, Department of Atmospheric Sciences, University of Wyoming, Laramie WY 82071, USA
email: geerts@uwyo.edu

Yet tornadoes can be quite intense in Wyoming. For instance, an F4 tornado caused significant property damage and one fatality in Cheyenne on 16 July 1979 (Parker and Hickey 1980).

Another F4 tornado, in the Teton-Yellowstone National Parks, displayed damage patterns of multiple vortices and microbursts (Fujita 1989). Evans and Johns (1996) described the antecedent synoptic conditions associated with three F2-F3 tornadoes in the Big Horn Mountains of north-central Wyoming. All these tornadoes occurred over terrain elevations >1832 m (6000 ft) MSL, in mid-summer (late June through early August), and under 500 hPa southwesterlies of weaker magnitude than the case herein. The present study is about a strong mesocyclone that became tornadic near a low-level baroclinic zone in southeastern Wyoming, over terrain above 2200 m MSL, rather early in the season

(22 May 2008), and under strong upper-level south-southeasterly flow. To our knowledge, a case like this has not been described in the formal literature, although it is not unprecedented, e.g. the similar 23 April 1960 Cheyenne Ridge tornado case described by Finch (2009).

This study explores the mesoscale aspects of the event, notably, the low-level thermodynamic and kinematic features that contributed to the evolution of a long-lived tornadic mesocyclone. The environment was rather unusual for a supercell. According to eyewitness reports, the tornado struck under cold (~7°C), foggy, yet windy surface conditions over the Laramie Range (elevation ~2500 m, see Fig. 1). Thus, without a dry layer below cloud base, convective cold-pool dynamics were likely of little significance in this case. Even though the boundary-layer air was saturated in the vicinity of the tornadic storm, its water vapor mixing ratio was at most 9 g kg^{-1}. CAPE in the inflow region was limited (<1000 J kg^{-1}). Supercells (and thunderstorms in general) are uncommon in environments with such low values of CAPE and mixing ratio (Brooks et al. 1994; Rasmussen and Blanchard 1998; Brooks et al. 2003b), but have been documented. For instance, Markowski and Straka (2000) report relatively shallow, rotating storms in an environment with strong low-level shear and CAPE ≤300 J kg^{-1}.

The purpose of this paper is to document an unusual tornadic mesocyclone, and to demonstrate the importance of the complex terrain in its formation and/or maintenance. In addition to operational data, mainly radar, we use high-resolution Weather Research and Forecasting (WRF) model simulations that reproduce the storm complex surprisingly well. The data sources and WRF setup are presented in Section 2. Section 3 analyzes the meso-α scale storm environment, and Section 4 describes the storm itself. Section 5 examines the vertical structure of stability and wind shear, and Section 6 speculates about the importance of vorticity banners in mesocyclone formation.

2. Data sources and model setup

a. Observations

This study uses visible and infrared satellite imagery, as well as the Cheyenne (KCYS) WSR-88D Level II and III products, available from the National Climatic Data Center (NCDC). The radar operated in Volume Coverage Pattern (VCP) 11 during the time of interest, with a temporal resolution of 5 min.

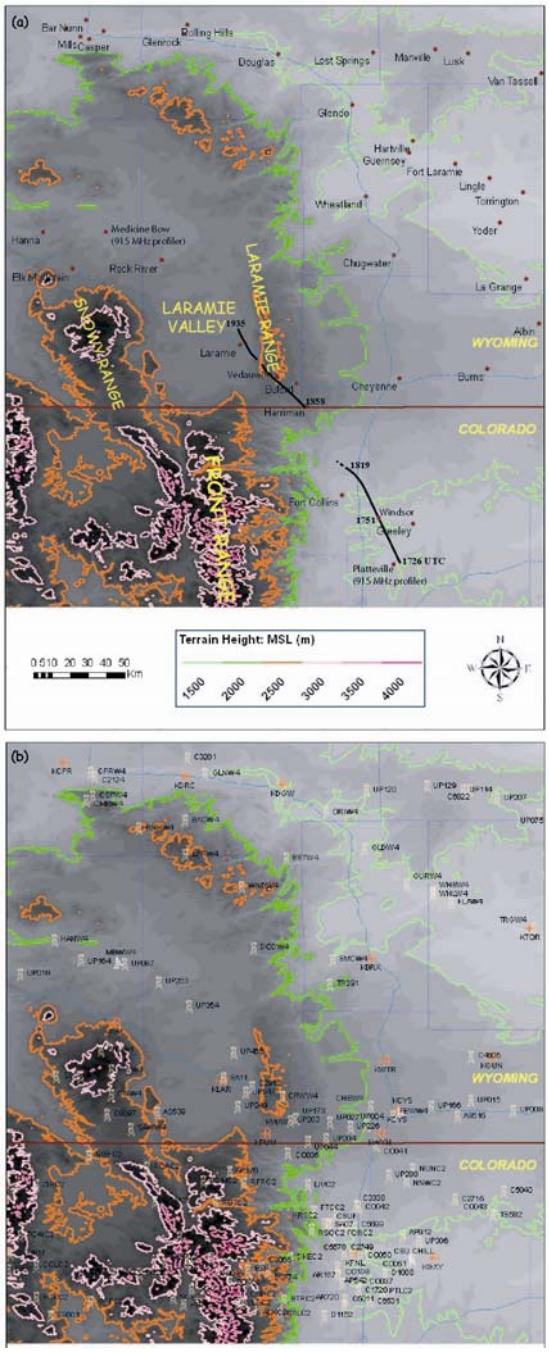

Figure 1: (a) Topography, state and county boundaries, interstate highways, and cities in the inner (meso-β scale) domain of the WRF simulation. Terrain elevation is shaded and color-contoured at 500 m intervals. Black paths denote tracks of 22 May 2008 tornadoes near Windsor, CO and Laramie, WY, based on a National Weather Service (NWS) damage survey and eyewitnesses (Finch and Bikos 2009). b) As in (a), but with the all *Mesowest* station locations shown as towers (non-METAR) or airports (METAR), and the location of the KCYS and CSU CHILL radars (radar symbol). Click image to enlarge.

WSR-88D level III products include algorithm-identified mesocyclones and tornado vortex signatures (TVS) (Mitchell et al. 1998). The 22 May 2008 mesocyclone moved from the southwest quadrant of the KCYS radar toward the northwest at a range increasing from 44 to 93 km. We also use data from the CHILL Doppler radar, a National Science Foundation facility operated by Colorado State University (CSU) and located about 45 km south of Cheyenne. The CHILL radar is similar to the WSR-88D (10 cm wavelength, ~1° beamwidth). During the time of interest it operated in rapid-scan (~1 min interval) single elevation angle (1.36°) mode.

The University of Utah Mesowest collects meteorological observations across the western United States (Horel et al. 2002). The area of interest is rather data-sparse. This study uses 35 to 45 *Mesowest* sites in the meso-β domain (Fig. 1) reporting at 5-60 min intervals. The data shown here are plotted at 30 min intervals, using data averaged over ±30 min. Station variables are displayed using the standard meteorological convention, and also are interpolated spatially onto a grid using Inverse Distance Weight (IDW) scheme available in the ESRI ArcGIS Spatial Analyst mapping software. Other data, including topography, are mapped onto the same grid using the same Geographic Information Systems (GIS) software. A combination of proximity data (nearby stations and nearby days), the terrain, and model output was used to determine subjectively whether data outliers are real or suffered some instrument- or site-related bias, in which case the data point is eliminated. The nearest radiosonde sounding is from Denver/Stapleton (DNR) at 1800 UTC, about the time of storm formation, but DNR is rather far from where the mesocyclone formed, ~105 km farther north. We also examined commercial aircraft take-off and landing soundings [using ARINC Communications, Addressing, and Reporting System (ACARS) data], but these too were centered near Denver. Continuous wind profiles from the Medicine Bow, WY 915 MHz wind profiler (Fig. 1a) were used, but the radar wind profiler at Platteville, CO (Fig. 1a) was inoperative on this ay. Finally, we use meteorological data from two communications towers near the path of the tornado.

b. Model data and numerical experiments

Output from the National Center for Environmental Prediction (NCEP) 4 km WRF-Nonhydrostatic Mesoscale Model (hereafter WRF-NMM) over the western USA is used to examine the meso-α scale conditions. This model was initialized at 0600 UTC only, about 12 hours before the event. Initial data from the 1800 UTC initialized 12 km NCEP North American Mesoscale (NAM) model (the operational WRF) are used as well. Model output is displayed using UCAR/Unidata's Integrated Data Viewer (IDV) and NWS BUFKIT software.

We ran the Advanced Research WRF (ARW, after Skamarock et al. 2008) version 3.0.1, with initial and boundary conditions provided by the hourly WRF-NMM data, initialized at 0600 UTC 22 May 2008. A nested grid was used, with the inner (1.33 km resolution) and outer (4 km resolution) domains in two-way interaction. We used the Lin et al. (1983) bulk microphysics scheme, including graupel, and the MYJ (Mellor Yamada Janjić) boundary-layer scheme (Janjić 1996). Cumulus convection was not parameterized in either the inner or outer domains. The Noah land surface model (Ek et al. 2003) was used, including various effects of terrain slope and cloudiness on the local surface energy balance.

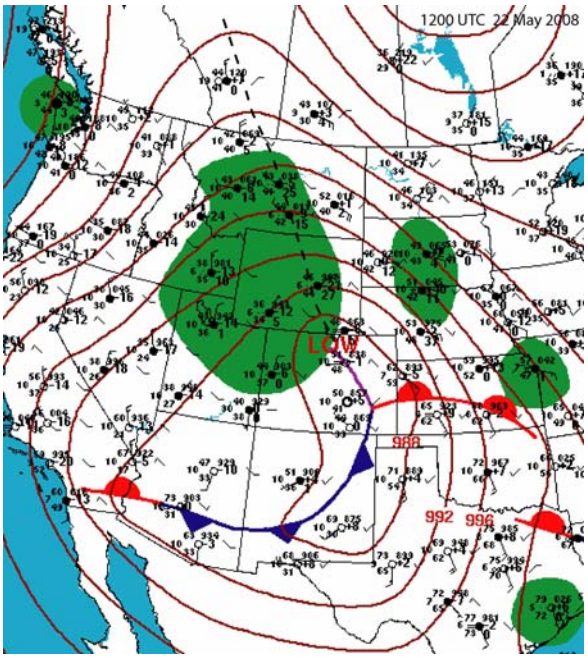

Figure 2: Hydrometeorological Prediction Center sea-level pressure and frontal analysis at 1200 UTC 22 May 2008. The green shading highlights the area with precipitation. We added the trough axis north-northwest of the low, as a dashed line.

3. Meso-α scale analysis

A low, with minimum sea-level pressure of 985 hPa centered over northeastern Colorado, dominated the surface circulation in the western USA (Fig. 2). Easterly flow north of a well-defined warm front advected relatively cool, moist air into southeastern Wyoming (Fig. 3). Surface flow gradually ascended

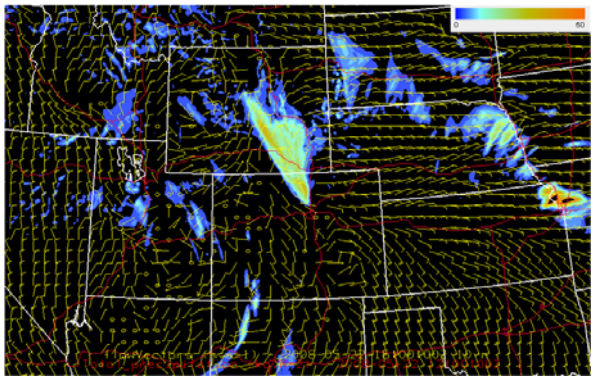

Figure 3: Surface wind barbs (full barb is 5 m s^{-1}) and 3 hour total precipitation (color fill, units mm, minimum plotted value 0.25 mm) at 1500 UTC 22 May 2008, from the WRF-NMM initialized at 6 UTC. Red lines are interstate freeways. Click image to enlarge.

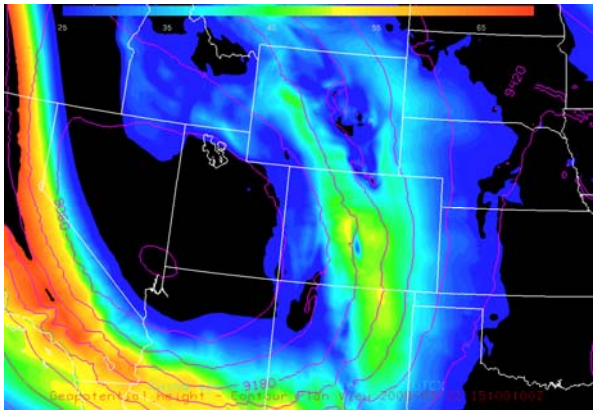

Figure 4: WRF-NMM 300 hPa height (magenta contours, 60 m interval) and isotachs (color fill, between 25-70 m s^{-1}) at 1500 UTC. Click image to enlarge.

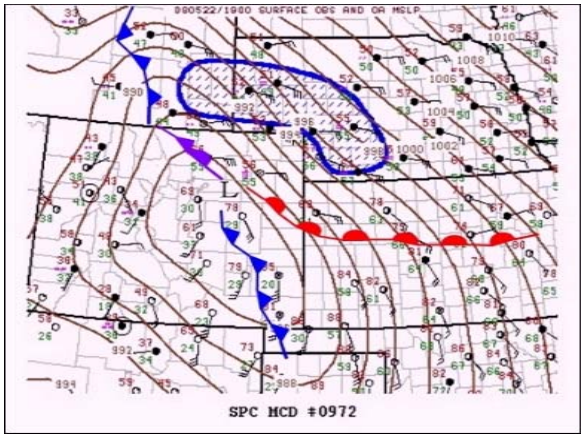

Figure 5: NOAA Storm Prediction Center (SPC) sea-level pressure analysis at 1900 UTC. Wyoming is in the upper left corner. The blue hatched shading highlights a region with strong low-level shear. Click image to enlarge.

over the central Great Plains, cooled, and became saturated near Cheyenne, in particular over the Laramie Range between Cheyenne and Laramie (Fig. 1). Early in the morning (1200 UTC), deep cloudiness and precipitation were widespread over Wyoming (Fig. 2). The surface low was associated with a deep, cut-off, 300 hPa low over the Intramountain Basin (Fig. 4).

Cut-off lows are not uncommon in this area, especially in spring, and the associated deep upslope flow north of the surface low can produce heavy precipitation in southeastern Wyoming (Boatman and Reinking 1984). The 22 May cut-off low was unusually intense, with the strongest 300 hPa winds on the upstream side. On the downstream side, a streak of high meridional momentum had advected northward early on 22 May, resulting in south to southeast wind peaking at 55 m s^{-1} over Colorado at 1500 UTC. A triangular region of weaker wind aloft over south-central Wyoming was carved into this jet streak (Fig. 4). This is probably due to convective transfer of weaker momentum from below; the WRF-NMM produced an area of heavy convective precipitation across this same area (Fig. 3).

While the cold front in southeastern Colorado (Fig. 2, Fig. 5) was frontolytic and became more defined as a dryline during the morning (Fig. 5), the warm front sharpened in northeastern Colorado and Kansas (Fig. 5), with a clear wind shift, a 5-10 K potential temperature (θ) drop (Fig. 6), and a well-defined radar fine line. Warm frontogenesis there occurred not only due to convergence and deformation, but also persistent stratus cover (and thus lack of boundary-layer heating) to the north, mainly over Nebraska (Fig. 5). For the period of storm development in southeastern Wyoming (18-2000 UTC), the warm front could have been analyzed as stationary. The cold-air wedge north of the warm front was rather shallow, resulting in strong shear between the surface and 700 hPa, mainly in the blue hatched region in Fig. 5. The highest low-level mixing ratio values were found in the warm sector, not so much ahead of the dryline (cold front), but rather along the warm front, where strong southeast flow advected low-level moisture from Kansas (Fig 6). The dryline moved toward the northeast, but remained south of the storm of interest.

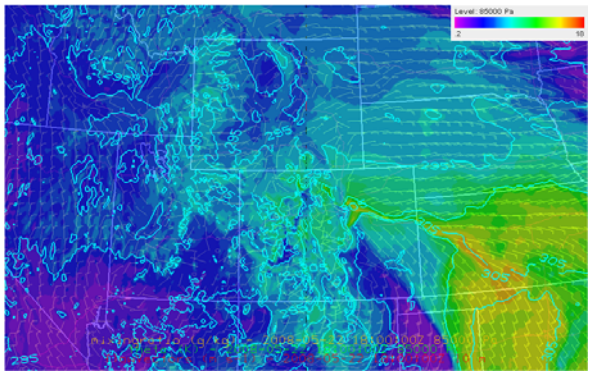

Figure 6: Surface winds (wind barbs), 850 hPa θ (cyan contours, 2.5 K interval) and 850 hPa mixing ratio (color fill, between 0.2 and 18 g kg^{-1}) at 1800 UTC, from the WRF-NMM. Click image to enlarge.

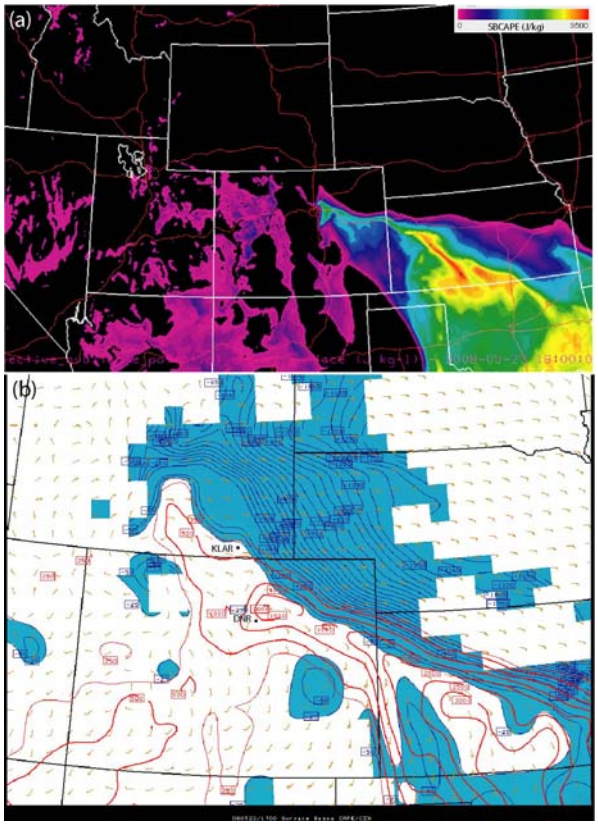

Figure 7: (a) SBCAPE (J kg^{-1}) at 1800 UTC from the WRF-NMM. (b) 1800 UTC SPC mesoscale analysis of SBCAPE (red contours, interval 500 J kg^{-1}) and SBCIN (blue contours, interval 50 J kg^{-1}), shaded blue where SBCIN <-25 J kg^{-1}. Click image to enlarge.

The highest CAPE values at 1800 UTC were close to the warm front in western Kansas (Fig. 7a). A sliver of high surface-based CAPE (SBCAPE), up to 1500 J kg^{-1}, was evident just south of the warm front from western Kansas to Denver, Colorado. (Denver is located at the intersection of several interstate freeways shown as red lines in Fig. 7a.) The WRF-NMM did not produce any SBCAPE in southeastern Wyoming at 1800 UTC (Fig. 7a) or at any time later that day, but the 1800 UTC SPC mesoscale analysis, based on an hourly synthesis of Rapid Update Cycle (RUC) initialization and surface observations (Bothwell et al. 2002), suggests SBCAPE ~500 J kg^{-1} near the Wyoming-Colorado state line just south of Laramie. Surface-based convective inhibition (SBCIN) became very large north of the warm front (Fig. 7b). The rate of change of SBCIN is an indicator of the temperature contrast across the warm front. According to the SPC analysis, this contrast was large in northeastern Colorado but smaller near Laramie. Laramie was barely within a region lacking substantial SBCIN. This suggests that the supercell remained surface-based as it moved over the warm front and approached Laramie.

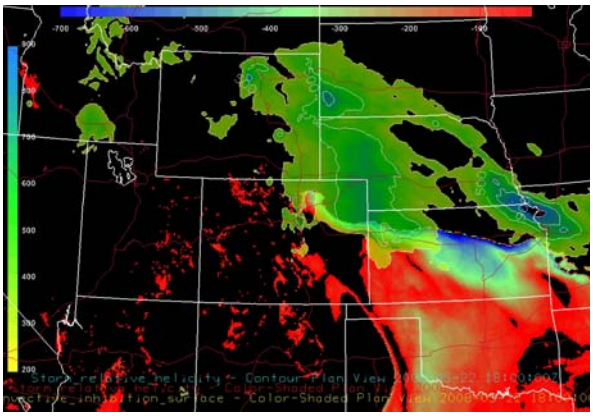

Figure 8: SBCIN (J kg^{-1}) in regions with non-zero SBCAPE, and 0-1500 m AGL SRH (m^2 s^{-2}) at 1800 UTC from the WRF-NMM. The key to SBCIN is on top (-700 <CIN< -25 J kg^{-1}), and the key to SRH (300 <SRH< 900 m^2 s^{-2}) is at left, with white contours every 200 m^2 s^{-2}. Click image to enlarge.

Modeled low-level SRH was highest just north of the warm front (Fig. 8), exceeding 500 m^2 s^{-2} in western Nebraska and northeastern Colorado. The WRF-NMM produced a secondary SRH maximum around Cheyenne (located at the intersection of interstate freeways in southeastern Wyoming in Fig. 8), with a peak value of 440 m^2 s^{-2}. Note that the integral bounds for the SRH shown in Fig. 8 are surface to 1.5 km AGL. Upper bounds of 3 km and 1 km are used more commonly (e.g. Markowski et al. 1998). We used an upper bound of 1.5 km AGL because only this SRH field was available in the NCEP WRF-NMM and 12 km NAM products.

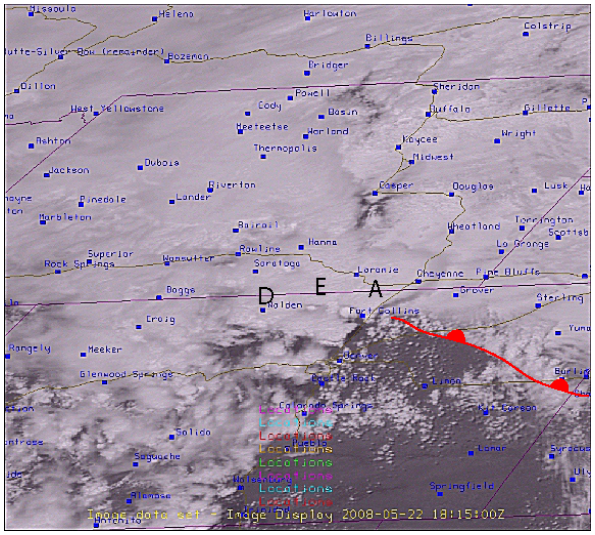

Figure 9: NOAA GOES visible satellite imagery over Colorado and Wyoming, with frontal analysis at 1815 UTC. Click here to view an animation from 1700 to 2000 UTC. Click image to enlarge.

4. Meso-β scale analysis

a. Satellite imagery

Widespread cloudiness persisted in the morning over Wyoming (Fig. 9). Infrared imagery (not shown) shows a region of high cloud tops in the shape of an inverted triangle from Laramie northward, consistent with the WRF-NMM precipitation field (Fig. 3). A stratus deck existed north of the quasistationary warm front (Fig. 9). Shallow convection developed in the warm sector wedge in eastern Colorado as early at 1700 UTC, especially at its northern edge where the air was more moist (Fig. 6). Deep convection developed over the warm front in far northeastern Colorado starting at 1815 UTC, with at least two spreading anvils near Yuma. We focus on the deep convection north of Denver in the first image of the animation at 1702 UTC (labeled 'A' in Fig. 9). Over the next hour this storm moved toward the north-northwest, intensified as evident from a rapidly-spreading anvil, and produced an EF3 tornado at Windsor CO, located 18 km southeast of Fort Collins CO, at 1751 UTC (Fig. 1). Another thunderstorm already had developed at 1702 UTC over the Front Range (labeled 'D' in Fig. 9). By 1745 UTC, a new storm (labeled 'E') had formed between 'A' and 'D', and by 1815 UTC the anvils of storms 'A', 'D', and 'E' had merged entirely. The eastern edge of the anvil of this mesoscale convective system remains visible in the next two hours as a darker shade between Cheyenne and Laramie, representing the anvil's shadow on the stratus deck. The anvil hides storm 'A' (defined by radar imagery, see below), which produced a tornadic mesocyclone near Laramie between 1830-2000 UTC. The anvil's minimum GOES-12 infrared brightness temperature within 10 km of storm 'A' decreased until 1915 UTC, at which time the KCYS-identified mesocyclone was also deepest (see below), and the cloud top height was 14 km MSL.

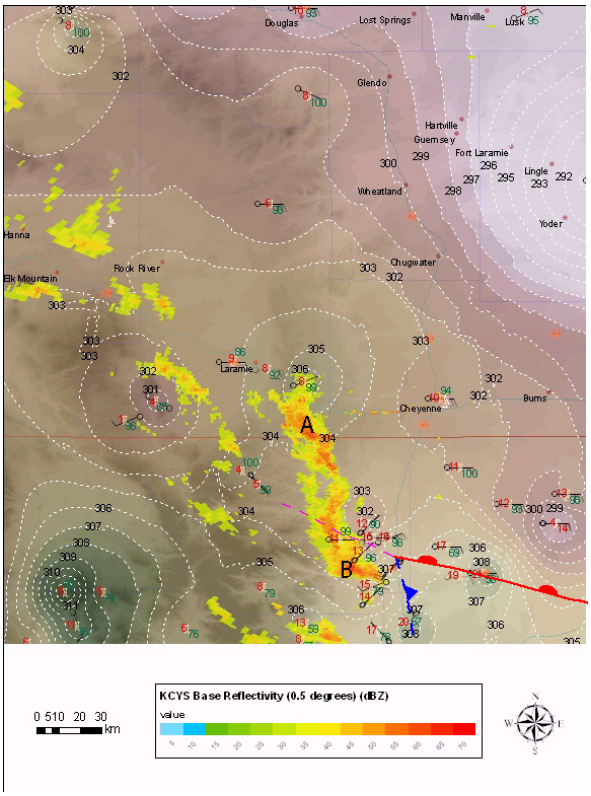

Figure 10: Objectively interpolated, observed θ (colored and contoured, 1K interval) and KCYS 0.5° radar reflectivity (colors in legend) over a terrain background (shading) at 1900 UTC. The temperature (red numbers), relative humidity (green numbers), and wind (one full barb is 5 m s^{-1}) are shown at each station, where available. Click here for an animation between 1800-2000 UTC. Click image to enlarge.

b. Surface observations

Detailed analyses and IDW interpolations of observed surface θ and equivalent potential temperature (θ_e) are shown with radar reflectivity between 1800-2000 UTC, in Figs. 10 and 11 respectively. Data distribution is quite uneven, with a wealth of reports near Fort Collins but a relative scarcity in Wyoming. Many stations do not report pressure, which is inferred hydrostatically from nearby stations with pressure data. θ is used because of the significant differences in station elevation.

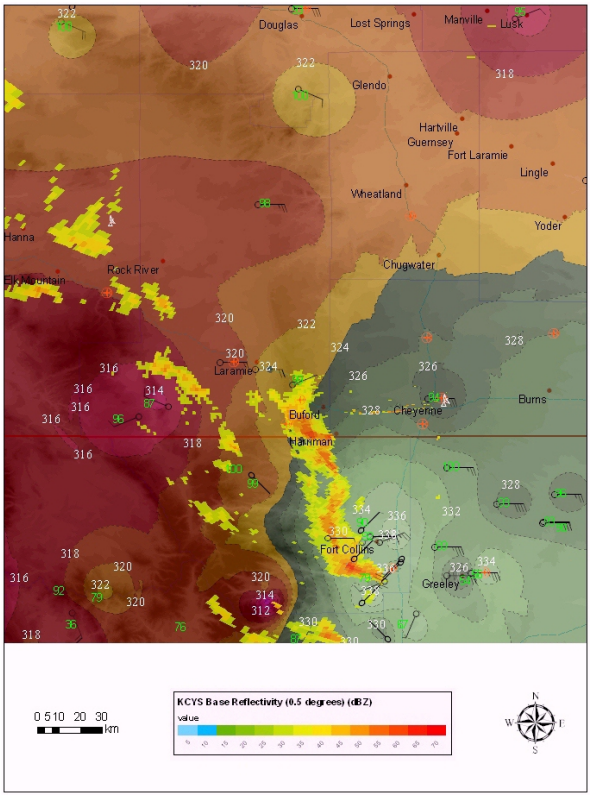

Figure 11: Objectively interpolated observed θ_e (colored and contoured, 2 K interval) and KCYS 0.5° radar reflectivity (warm colors) over a terrain background (shading) at 1900 UTC. The relative humidity (green numbers) and wind barbs are shown at each station, where available. Click here for an animation between 1800-2000 UTC.

During the same two-hour period, it remained considerably cooler toward the northeast of the domain in Fig. 10, on the cold side of the warm front. The frontal analysis in Fig. 5 is extended to the smaller domain of Fig. 10. The θ_e values decrease toward the northwest (Fig. 11), with a clear maximum just east of the Front Range in the vicinity of Windsor, where storm 'A' spawned an EF3 tornado (Fig. 1). This is consistent with the SBCAPE maximum in this area (Fig. 7b). The region of high θ_e moves north slightly between 1800-2000 UTC, but more slowly than the storm complex. Also, the θ_e gradient across the warm front is small compared to the θ gradient, since the drop in temperature is somewhat offset by an increase in humidity.

The warm-frontal location in Fig. 10 is based on a fine line clearly present in 0.5° radar reflectivity imagery from the Denver WSR-88D and the CHILL radars. Such fine lines result from convergent flow in the convective boundary layer (Wilson et al. 1994; Geerts and Miao 2005). This feature was defined best in eastern Colorado, but vanished near Windsor (Fig. 1) at 1830 UTC, following the passage of storm 'A'. The objectively drawn isentropes do not line up with the warm front; but on a larger scale, the backed wind, increase of humidity, and θ drop (Fig. 10) across the fine line confirm that it was the warm front. The cold and occluded fronts lacked the boundary-layer convergence necessary to reveal radar reflectivity fine lines.

At 1800 UTC, storm 'A' was surrounded by a convective cold pool. Relatively warm air was found around the southern Laramie Range (e.g., at Vedauwoo, KVDW in Fig. 1), even though this range was north of the warm front. Vedauwoo is at an elevation of 2560 m MSL, >1000 m higher than Fort Collins. Several data sources confirm that the higher terrain near Vedauwoo, where storm 'A' passed at about 1900 UTC, was engulfed by the cold air north of the warm front. It appears that the warm front was not very shallow. The Medicine Bow 915 MHz wind profiler (location shown in Fig. 1a) revealed some 2-3 km AGL veering with height from east to southeast between 1700-2000 UTC, suggesting that the warm (or occluded) front was at 4-5 km MSL there. Stations in the southwest quadrant of Fig. 10 reported southwest winds and relatively high θ, suggesting that they remained sheltered from the cold airmass by the Front Range. The Laramie Range, therefore, did not block the easterly pre-frontal flow, while the higher Front Range did. Strong easterly surface flow (7-16 m s^{-1}) was found at Cheyenne, Vedauwoo and Laramie between 1800-2000 UTC. This easterly current apparently mixed with the warm-sector air above, especially over the Laramie Range, due to turbulent mixing in the 700-1000 m deep boundary layer (depth inferred from WRF-NMM soundings). Despite the stratus deck, the mixing was aided by surface heating near local solar noon (at 1858 UTC).

The warm front sharpened toward 2000 UTC, with warm southwesterly flow in the Fort Collins – Denver area and cooler, more humid easterly flow north of the front (Fig. 10). Stations generally recorded easterly to northeasterly wind alongside the storm complex (shown as radar echoes in Fig. 10) as the latter progressed northward. The surface flow supplying the storm complex was nearly saturated: the relative humidity in Cheyenne remained over 90% between 1800-2000 UTC, and fog was present at Vedauwoo and elsewhere near the Laramie Range crest, according to station and eyewitness reports.

In summary, warm-sector inflow was available for storm 'A' until about 1800 UTC. Afterward, its inflow became increasingly mixed with more humid,

colder, and more stable (lower θ_e) air, i.e., with the cold airmass north of the warm front, as the storm travelled north over the warm front and gradually higher terrain. The inflow became saturated as it was lifted over the terrain. Analyses of the surface θ and θ_e suggest that storm 'A' did not decouple from the surface to become "elevated" convection (Horgan et al. 2007), at least not before crossing the Laramie Range. The easterly inflow into storm 'A' had steady surface θ between 302-304 K (Fig. 10) as the storm moved north of the warm front. The θ_e of the surface air for storm 'A' did decrease from ~330 K to ~320 K between 1800-2000 UTC (Fig. 11), consistent with the decrease in SBCAPE along the track (Fig. 7b). More evidence for surface-based convection will follow later when we examine soundings.

c. Radar reflectivity

The movie loop of the 0.5° KCYS radar reflectivity (Fig. 12a) depicts the evolution of the storm system. Note that the beam remains very close to the terrain east of KCYS, all the way to the crest of the Laramie Range; some ground clutter exists near the crest (Wolfe et al. 2008). Strong echoes (and large Doppler velocities) were common along a narrow ribbon between KCYS and the crest, attributed to vehicles on the I-80 freeway. The CHILL radar, located 131 km southeast of Laramie near Greeley (Fig. 1b), operated in rapid-scan, constant-elevation mode (Fig. 12b). Widespread precipitation with some embedded convection, and with cloud tops around 12-13 km MSL, was present west of Laramie at 1830 UTC. The precipitation remained there for the next two hours, produced by storms moving off the Front Range, starting with storms 'D' and 'E' (Fig. 9). We focus on storms 'A' and 'B' (Fig. 12a), both elongated with anvils of lighter precipitation directed toward the north-northwest. Storm 'A' had been tornadic (at Windsor, CO) until 1819 UTC (Fig. 1). The precipitation fields of storms 'A' and 'B' merged around 1900 UTC into a large, elongated storm system just south of the WY-CO state line. This linear complex contained several convective cells, with the CHILL radar reflectivity exceeding 65 dBZ in the two northernmost cells ('A' and 'C') between 1900-1910 UTC and in cell 'B' between 1910-1935 UTC (Fig. 12b). Large hail was reported from cells 'B' and 'C'. The CHILL reflectivity animation shows that the warm-frontal fine-line was quasistationary (Fig. 12b). Only when cell 'B' crossed the warm front did its peak reflectivity exceed 65 dBZ.

Storm 'A' ascended the Laramie Range at 19-20 m s^{-1}. During 45 min the underlying terrain rose by ~1000 m. Thus, even though θ_e decreased along

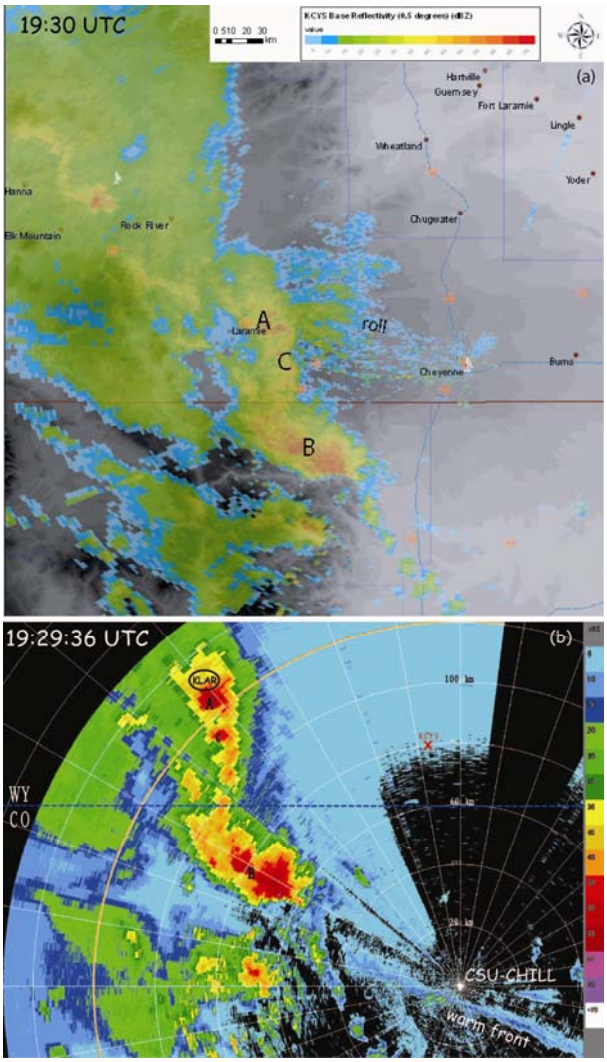

Figure 12: (a) KCYS WSR-88D base reflectivity (0.5° elevation) (dBZ) at 1930 UTC. Click here for an animation between 1830-2000 UTC. (b) CSU CHILL base reflectivity (0.5° elevation) (dBZ) at the same time. Click here for an 1830-2000 UTC animation. Range rings are plotted every 20 km. The black oval locates Laramie.

its track (Fig. 11), storm 'A' re-invigorated, with increasing peak reflectivity values toward 1900 UTC, at which time it had spawned a second tornado near the Wyoming-Colorado state line (Fig. 1). Cyclonic rotation and hook echo formation are evident in cell 'A' from 1930-1950 UTC (Fig. 12a). There were several zonal, narrow echo bands east of the Laramie Range (labeled 'roll' in Fig. 12a). These were absent in higher-elevation KCYS scans, thus they were shallow. They first intersected the eastern edge of storm 'A' at 1921 UTC, when the storm moved over the crest of the Laramie Range. As the bands advected to the northwest and became more defined, they also appeared to rotate slightly clockwise,

maybe because of strong southeasterly flow in the wake of storm 'A'. The bands may have been the result of horizontal roll circulations in the sheared convective boundary layer. The transient nature of such rolls may be due to the temporarily more intense wind shear as the storm complex passed through. Such features can aid in supercell development (Thompson and Edwards 2000) and have been associated with supercellular tornadogenesis near complex terrain (e.g., Elson et al. 2008).

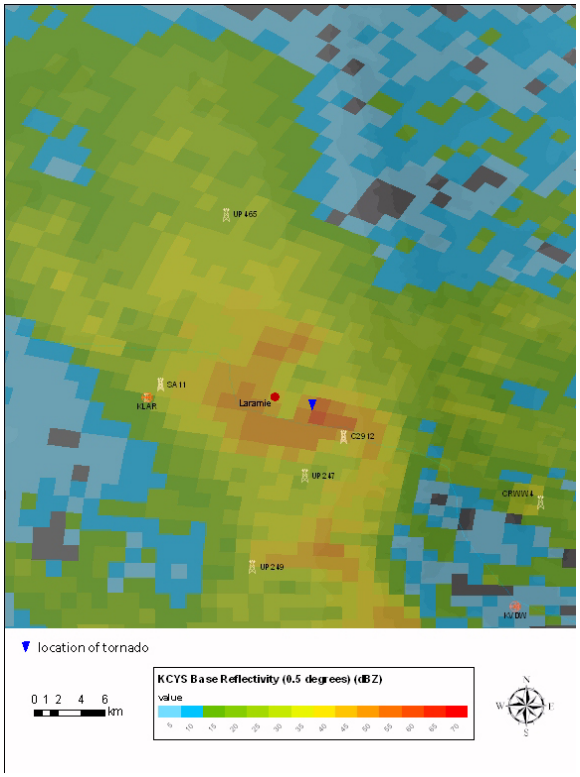

Figure 13: 1930 UTC KCYS radar reflectivity near Laramie, when the tornado struck the southeastern edge of Laramie. Click here for displays at increasing elevation angles. The height of the radar beam above Laramie is 1.2 km at 0.5°, 2.4 km at 1.5°, 3.5 km at 2.4°, and 4.7 km at 3.4°. The blue triangle marks the location of the tornado at the surface. Click to enlarge.

A zoomed 1930 UTC view of storm 'A' reveals a 50-60 dBZ reflectivity core tilting northwestward with height, consistent with ambient southeast shear (Fig. 13). A large hook echo, covering ~4 km^2, is most evident in the 0.5° scan. A tornado was present near the leading edge of the hook (Fig. 13). The hook's orientation, and the unusual position of the weak echo region (WER) on the northeast side of the shell of maximum reflectivity, is consistent with textbook depictions of a supercell storm [e.g., Fig. 8.10 in Houze (1993)] if the east axis is rotated counterclockwise toward the north. This axial shift

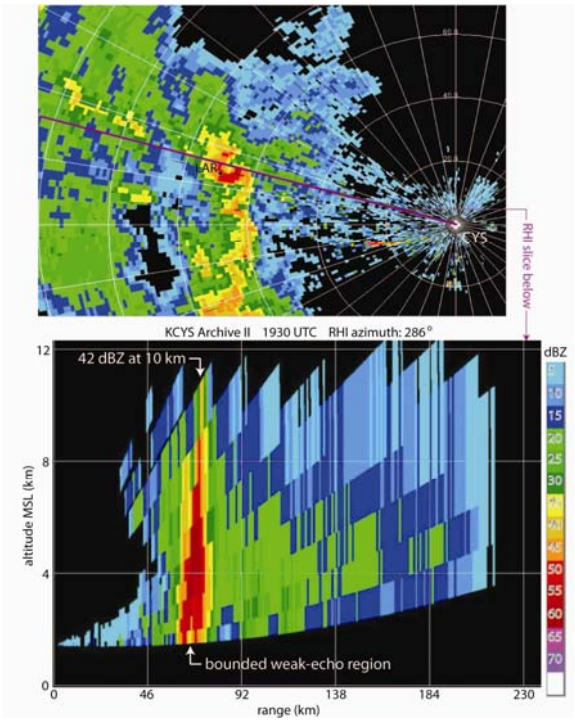

Figure 14: Vertical reflectivity slice from the KCYS WSR-88D radar at 1930 UTC, along an azimuth angle of 286° (purple line in insert image above). Click to image enlarge.

is consistent with the 0-6 km southeasterly mean wind. Storm 'A' likely contained strong updrafts, given the presence of a WER capped by a 42 dBZ echo at 10 km (Fig. 14). Yet compared to many Great Plains supercell storms, the storm top and WER were relatively shallow. The ceiling of the WER was just above the 1.5° elevation scan (~2.4 km AGL, Fig. 14).

d. Radar Doppler velocity

The KCYS storm-relative Doppler velocity at 0.5° is shown in Fig. 15. This is a Level III product, i.e., the velocities have been de-aliased by algorithm, based on two radial velocity estimates [dual pulse repetition frequency (PRF)], at least within the high-PRF maximum unambiguous range (148 km in this case) (e.g., Torres and Zrnic 2004). Many regions are range-folded. Some discontinuities are still present, not surprising given the highly sheared flow. Some velocity jumps along radials appear to be twice the maximum unambiguous velocity (twice 9 m s^{-1}, or 28 m s^{-1} for the two PRFs in this case). We tried to overcome the algorithmic troubles by manually unfolding select areas in the Level-II (raw) velocity displays using UCAR solii software. In some regions, the radial flow became more plausible, but the Level-III product was better overall, thus we

examine the Level-III base and storm-relative velocities. The latter removes the storm motion, defined as the average of all storm motion vectors in the "storm track information" product. During the period of interest the storm motion was ~16 m s^{-1} toward 328°. We display the storm-relative velocity (Fig. 15) because it better reveals the mesocyclone.

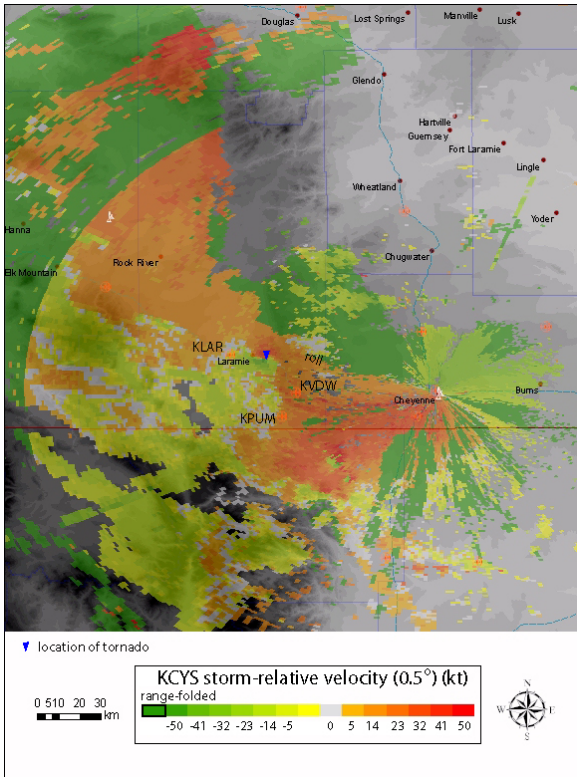

Figure 15: KCYS WSR-88D storm-relative velocity (0.5° elevation) (kt) at 1930 UTC. Click here for an animation.

KCYS and KFTG (Denver) WSR-88D storm-relative velocity data indicate that the first mesocyclone in storm 'A' (the Windsor storm) disappeared at about 1818 UTC (not shown). Strong near-surface north-easterly storm-relative flow (>20 m s^{-1}) was present between KCYS and storm 'A' from 1830-1850 UTC, as the storm ascended toward the Laramie Range (Fig. 15). The ground-relative flow was from the east rather than the northeast. The storm-relative flow was exceptionally strong (>50 kts) in the oval highlighted in Fig. 15 at 1830 UTC. An identical inbound jet on the northeastern side of KCYS is absent, so it must be a local jet. This near-surface easterly jet is located in an orographic saddle between the Laramie Range and the Front Range near the WY-CO state line (Fig. 1), suggesting that the jet was channeled into the terrain gap and connected with the developing mesocyclone (highlighted with a black arrow in Fig. 15). The easterly jet intensified as mesocyclone 'A' approached, but it was present already when storm 'A' was still remote, between 1730-1830 UTC (not shown); therefore, the jet started as a gap current and was not merely a response to the convection. Also, strong flow persisted across the saddle after storm 'A' had passed. Initially, storm 'A' inflow was more convergent than cyclonic (Brown and Wood 1991), especially at 1850 UTC, but by 1900 UTC the mesocyclone was clearly established, and it continued to be evident at increasing radar range until 2000 UTC.

The inflow of storm 'A' veered slightly as the storm approached Laramie. Ribbons of weaker and stronger outbound flow alternated over the Laramie Range, mainly between 1930-2000 UTC (Fig. 15). The orientation and wavelength of the velocity variations match those in the reflectivity (Fig. 12), thus the easterly flow was modulated by the roll convection discussed above. While storm 'A' produced a strong mesocyclone, several other weaker mesocyclones were identified by algorithm, e.g. storm 'B' at 1951 UTC just southeast of KPUM (Pumpkin Vine) (Fig. 15).

The mesocyclone in storm 'A' was quite broad at maturity, with a diameter of ~10 km (Fig. 16), and tilted northwestward with height due to ambient wind shear. It was strongest near the surface, but evident

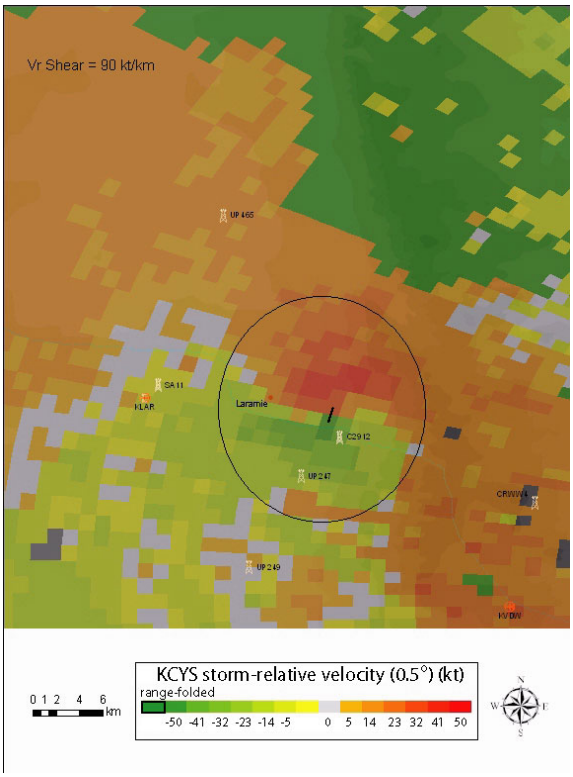

Figure 16: As in Fig. 15, but zoomed to the Laramie vicinity. Click here for displays at increasing elevation angles.

at all elevations up to the highest angle with echo (~10 km AGL). At the lowest angle (0.5°) the strongest radial velocity shear between adjacent beams was 46 m s^{-1} km^{-1} at 1930 UTC (Fig. 16). While this strong beam-to-beam cyclonic shear decreased with height, it resulted in a TVS identification at all levels up to 8 km AGL.

e. The tornado

Storm 'A' spawned a tornado at 1858 UTC at the WY-CO state line near Harriman (UP044, see location in Fig. 1). Finch and Bikos (2009) surveyed the path in the summer of 2008, providing numerous photographs of damage rated up to EF2. There are several sections on the path toward Laramie where the evidence is inconclusive, not surprising given the lack of trees or manmade structures on the Laramie Range. It is unclear whether there was a single, persistent tornado between Harriman and Laramie, or successive ones. No verifiable photo of the tornado is available, even from when it crossed east Laramie between 1928-1935 UTC. Eyewitnesses reported a broad, rotating wall cloud near the surface.

KCYS radar data continuously identified the TVS in storm 'A' from 1830-1951 UTC (Fig. 17). In each volume sample, this TVS was strongest in the lowest scan (0.5°). Its track matched the tornado damage path between Harriman and Laramie (Fig. 1). The TVS deepened as the parent storm ascended the Laramie Range (Fig. 18). In two radar volumes, the TVS and echo tops corresponded at ~10 km. After crossing the terrain ridge around 1920 UTC, the TVS top declined to ~7 km AGL. There is no evidence of spin-down (vertical vortex contraction) during the ~1000 m terrain ascent between 1830-1918 UTC, nor is there evidence of a spin-up (vortex stretching) during the ~500 m terrain descent between 1918-2000 UTC (Fig. 19). Instead, the maximum cyclonic shear in the TVS increased as the mesocyclone approached the terrain ridge, and decreased after 1904 UTC. The TVS was closest to KCYS at 1904 UTC, and its radar range increased rapidly after 1930 UTC. A rotational wind shear of up to 84 m s^{-1} km^{-1} (Fig. 19) is extremely high. Even the 46 m s^{-1} km^{-1} value (resulting from a 45 m s^{-1} velocity difference between adjacent beams, Fig. 16) at 1930 UTC, when the tornado hit Laramie, is likely to be associated with a tornado (e.g., Vasiloff 1992).

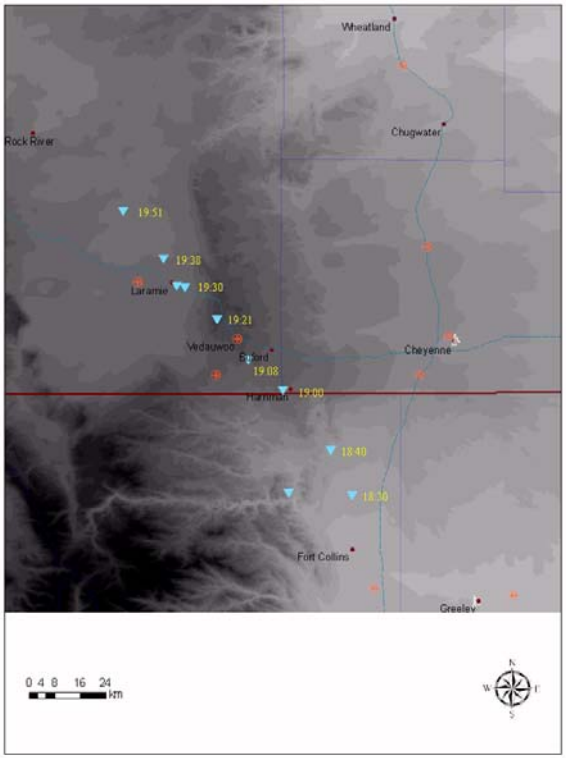

Figure 17: Track of the KCYS radar-detected TVS in storm 'A' (blue triangles), UTC times in yellow. Click image to enlarge.

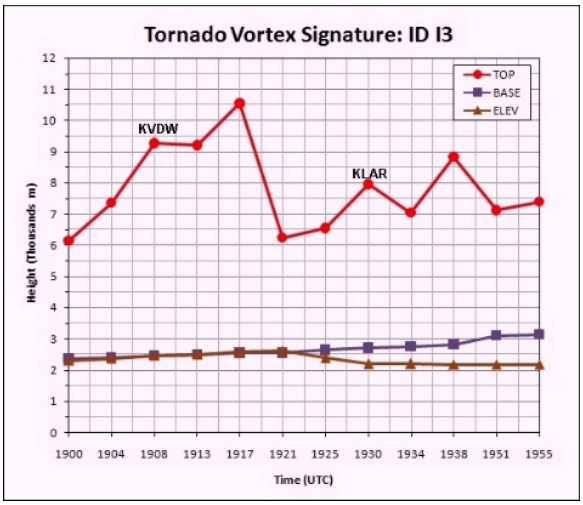

Figure 18: Evolution of the echo top and echo base of the TVS in storm 'A'. The brown line indicates the height of the underlying terrain. Click image to enlarge.

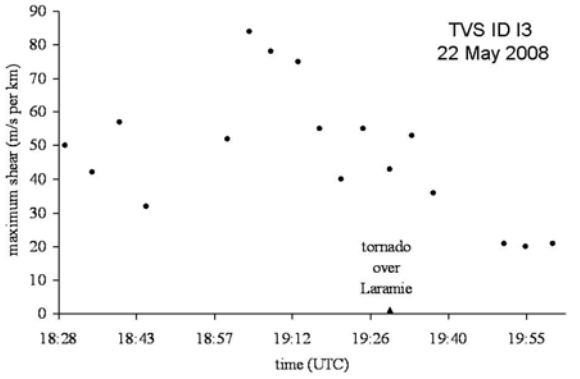

Figure 19: Evolution of maximum cyclonic shear of the TVS in storm 'A', based on KCYS Level II radial velocity data at any elevation angle. Click image to enlarge.

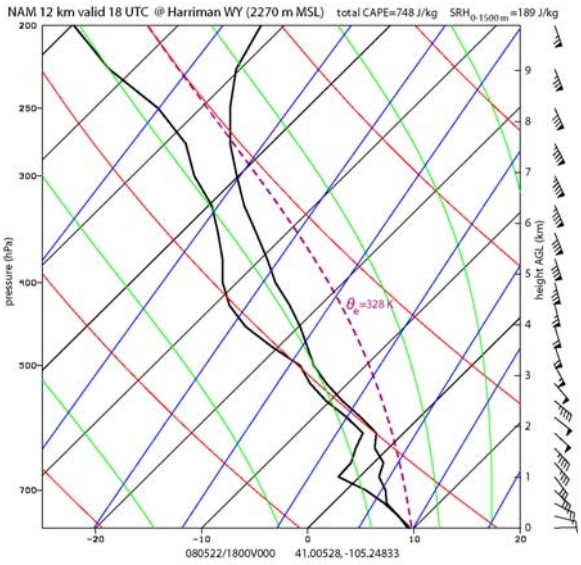

Figure 20: Model sounding from the 12 km NAM (initialized at 1800 UTC) at the location of Harriman (Fig. 1) at 1800 UTC. Click image to enlarge.

5. Sounding analysis

a. Stability

Model and proximity radiosonde soundings were analyzed to examine the stability near storm 'A'. We chose the site of Harriman to characterize storm inflow at the time of tornadogenesis because it was just east of the mesocyclone track at 1858 UTC (Fig 1). The 12 km NAM sounding at Harriman had a SBCAPE value of 748 J kg^{-1} at the model initial time (1800 UTC) (Fig. 20). [Our calculation of SBCAPE includes the virtual temperature correction (Doswell and Rasmussen 1994).] This sounding (Fig. 20) is remarkable, not because of the absence of any CIN, but because air in the lowest 600 m AGL is eminently unstable. In fact the 12 km NAM produced convective precipitation over and downstream of Harriman in the first hour.

The sounding appears to be representative, and the location of Harriman has the deepest layer of moist absolute instability in the surrounding area. The model surface θ_e value is 328.1 K, very close to the 327.4 K value observed at Harriman at this time (Fig. 11). Also, the model sounding is quite similar to the modified 1800 UTC DNR sounding (Fig. 21). The DNR sounding was adjusted to remove data below the terrain elevation of Harriman, and to incorporate the temperature and dewpoint values observed at Harriman at its pressure level (756 hPa). We also modified this sounding for the Harriman surface wind and the overhead low-level wind from KCYS radar data. The adjustment layer was deep enough (75 hPa above Harriman) to avoid a superadiabatic lapse rate and to allow a smooth transition of all variables.

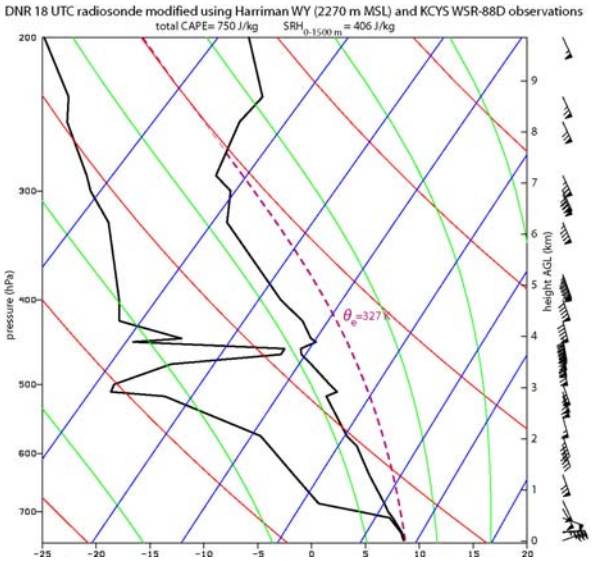

Figure 21: Observed Denver (DNR) sounding at 1800 UTC, modified with boundary-layer observations near Harriman at 1800 UTC. Click image to enlarge.

The modified 1800 UTC Denver sounding (Fig. 21) is much drier than the 12 km NAM sounding (Fig. 20) between 700-500 hPa, consistent with the model humidity gradient between Denver and Harriman in this layer, but it is similar to the model sounding in terms of instability, with SBCAPE of 750 J kg^{-1}. The SPC mesoscale analysis map has an SBCAPE of ~500 J kg^{-1} at Harriman at 1800 UTC (Fig. 7b). Thus we can be rather confident that the inflow region of storm 'A' near Harriman had an SBCAPE of 500-750 J kg^{-1}. The 12 km NAM (initialized at 1800 UTC) indicates that SBCAPE

quickly decreased north of Harriman along the mesocyclone track, consistent with the observed decrease of surface θ_e along the track (Fig. 11); the surface θ_e dropped from 329 K to 322 K between Harriman and Laramie at 1900 UTC. A surface θ_e of 322 K yields SBCAPE of just 81 J kg^{-1} in the modified 1800 UTC Denver sounding (Fig. 21).

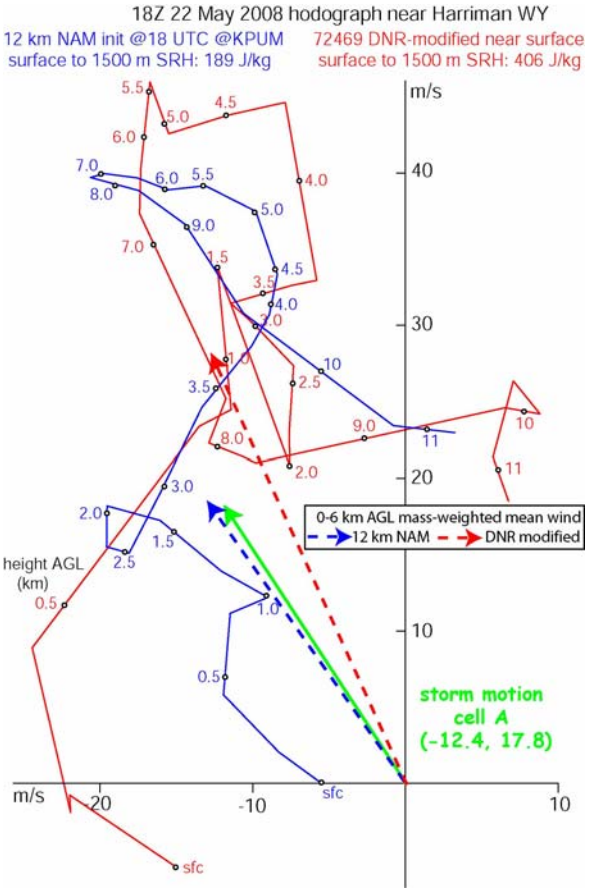

Figure 22: Two hodographs for Harriman at 1800 UTC. Red represents the 1800 UTC Denver radiosonde, modified as stated in the text. Blue represents the unmodified 12 km NAM initialized at 1800 UTC. Observed storm motion is in green. Click image to enlarge.

b. Wind shear

The vertical wind profile is marked by strong low-level shear and strong south-southeast winds above 700 hPa. 1800 UTC surface winds near Harriman in the 12 km NAM, initialized both at 1200 and at 1800 UTC, are east to southeasterly (e.g., Fig. 20). The WRF-NMM produces northeasterly wind at 1800 UTC, but at a speed of only 5-7 m s^{-1} (Fig. 6). The observed surface wind backed to the northeast between 1800-1900 UTC at several *Mesowest* locations, e.g., from 70° at Lynch (UP204) and 40° at Buford (UP 173, locations in Fig. 1), with an average speed of 17 m s^{-1} from 1800-1900 UTC. Low-level inflow for storm 'A' from the northeast was corroborated by data from a tower located near the Laramie Range ridge, just west of the tornado track (Fig. 1) and 5 km north of the WY-CO state line (Finch and Bikos 2009). The KCYS velocity-azimuth display wind profile, which is inferred from a 20 km radius circle centered at KCYS, does not capture any northeasterly wind between 1800-2000 UTC (not shown); the winds only back as far as 90° just before 1900 UTC, at a speed of 22 m s^{-1} at the lowest level. Nevertheless. a clear local east-northeast wind maximum was present in the 0.5° elevation KCYS base velocity pattern, in the gap south of the Laramie Range, between 1800-1830 UTC (Section 4d). In summary, we have high confidence that the 10 m winds near Harriman were from the east-northeast at 15-20 m s^{-1} as storm 'A' approached.

The presence of a northerly component in the strong easterly low-level winds (Fig. 21) is important because it significantly increases the SRH, compared to a situation with winds from the east to southeast, as the 12 km NAM predicted (Fig. 20). The WRF-NMM predicted a 0-1.5 km SRH of nearly 400 m^2 s^{-2} at 1800 UTC near Harriman, based on its forecast storm motion (Fig. 8). The 1800 UTC Denver radiosonde, modified with near-surface wind data as discussed above, yielded an SRH of 406 m^2 s^{-2} over the same depth (Fig. 21, Fig. 22). This estimate assumes the observed motion of storm 'A'.

Very strong low-level wind shear (e.g., 34 m s^{-1} within 1 km AGL) is evident in the modified Denver hodograph in Fig. 22. This certainly is sufficient for supercells (e.g., Weisman and Klemp 1984), especially since it occurred just above the level of free convection (Fig. 21), i.e., within the effective storm inflow layer (Thompson et al. 2007). However, the observed SBCAPE and near-surface mixing ratio (at most 9 g kg^{-1}) are rather low for supercell formation. In terms of the energy-helicity index [EHI (Hart and Korotky 1991), proportional to the product of SRH and CAPE], the storm environment fits with those of other tornadic storms (Fig. 23). The 22 May 2008 Laramie mesocyclone had a 0-3 km SRH estimated between 400-600 m^2 s^{-2}, and an SBCAPE initially up to 750 J kg^{-1} (although rapidly decreasing along the storm track). Thus the EHI was over 1.0, possibly over 2.5, during the mesocyclone formation period (1830-1900 UTC). Tornadic mesocyclones have been observed in environments of EHI <1.0 (Fig. 23).

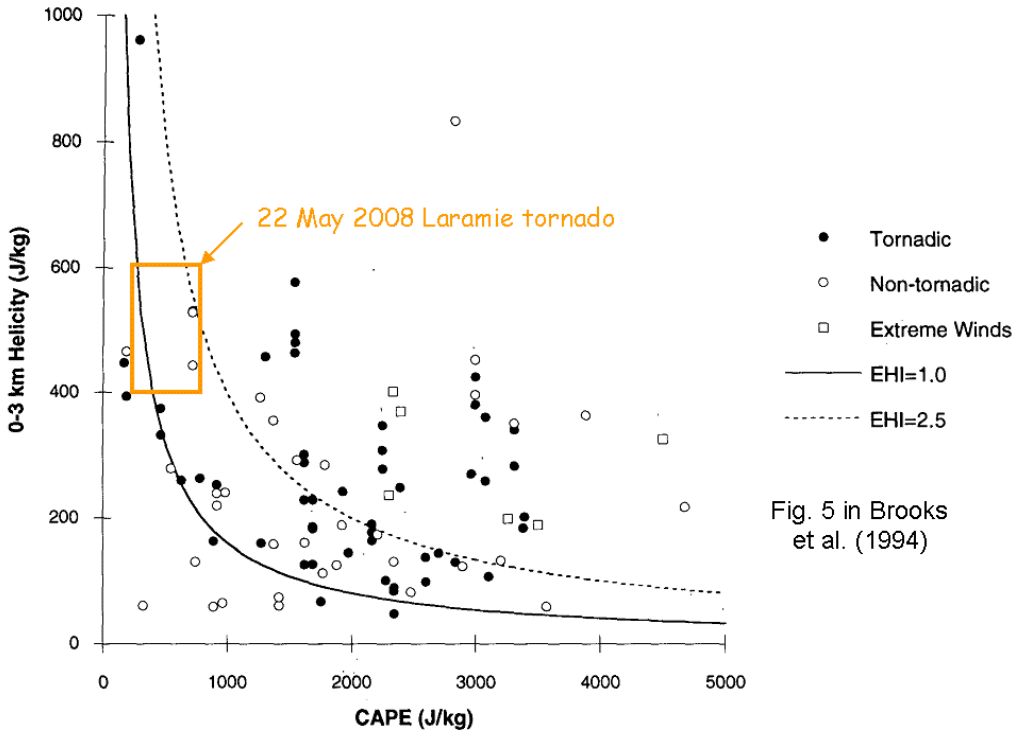

Figure 23: CAPE and 0-3 km SRH for the environment of the Laramie mesocyclone and of 112 mesocyclones, mostly in the central Great Plains [from Brooks et al. (1994)]. Energy-helicity index (EHI) isopleths of 1.0 and 2.5 are shown by a solid and a dashed line respectively.

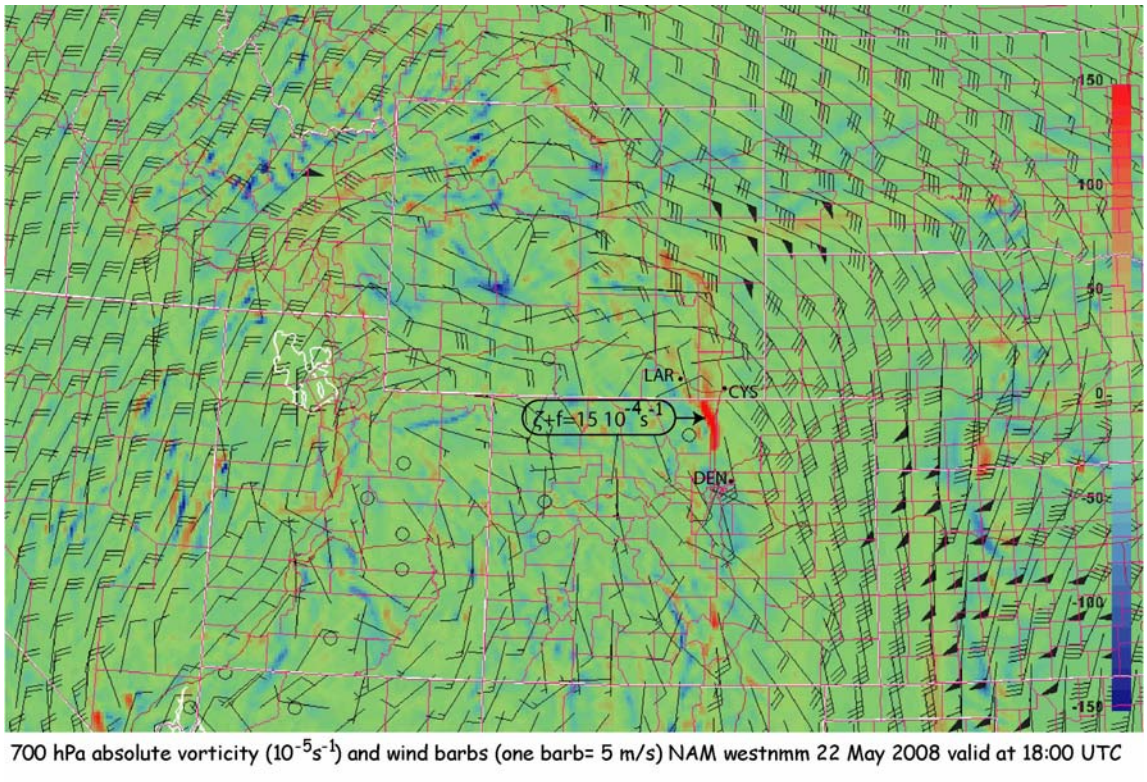

Figure 24: Absolute vorticity and wind at 700 hPa at 1800 UTC, according to the WRF-NMM. The location of Laramie (LAR), Cheyenne (CYS), and Denver (DEN)are highlighted.

The modified DNR wind profile near storm 'A' shows substantial low-level clockwise curvature between 0-1.5 km (Fig. 22). Right-moving supercells are supported by such a wind profile (Weisman and Klemp 1982). Storm 'A' (and other cells in the vicinity) moved slightly to the left of the 0-6 km mass-weighted mean wind in the modified Denver sounding (Fig. 22), yet slightly to the right of the same mean wind in the 12 km NAM sounding. Typically, the motion of right-moving supercells departs about 30° from the mean wind direction (e.g. Zeitler and Bunkers 2006), yet storm 'A' did not move significantly to the right of other storms in the vicinity, and there was no evidence that storm 'A', when it first formed around 1710 UTC, resulted from the splitting of a single initial storm. Environmental heterogeneity appears to explain the presence of mesocyclones moving with the deep-layer mean wind (and not to the right of it), as discussed next.

6. Orographically-generated potential vorticity banners and mesocyclone formation

We now examine the hypothesis that the tornadic mesocyclone near Harriman WY (and also the earlier one at Windsor, CO) *acquired some of its vertical vorticity from the mesoscale environment*. This hypothesis arose as we examined vorticity in the operational WRF-NMM. A lens of high cyclonic absolute vorticity, as high as 1.5×10^{-3} s^{-1}, was present between Denver and the WY-CO state line at 700 hPa (Fig. 24), only slightly weaker at 500 hPa. This value was much larger than observed anywhere else on Fig. 24. The observed shear vorticity of mesocyclone 'A' at 1930 UTC was about 50 m s^{-1} over 5 km, or 10^{-2} s^{-1} (Fig. 16), i.e., about one order of magnitude larger than the maximum value resolved by the 4 km WRF-NMM. Is it possible that the updraft of storm 'A' became mesocyclonic al least partly because it stretched the ambient vorticity, rather than only tilting horizontal vorticity associated with strong southerly shear (Fig. 22)?

Circumstantial evidence for this hypothesis comes from a WRF simulation at a resolution finer than the WRF-NMM (Fig. 25). The WRF architecture is discussed in Section 2b. First we examine whether the WRF was able to reproduce the convective storm complex in roughly the right time and place. The SBCAPE was much underestimated (Fig. 26), not surprising since the WRF initial and boundary conditions came from the WRF-NMM (initialized at 0600 UTC), and it also underestimated SBCAPE near Harriman (Fig. 7). Given the lack of CAPE, it may be surprising that convection occurred in the WRF inner domain, in roughly the right location but 1-2 hours delayed compared to observations. The

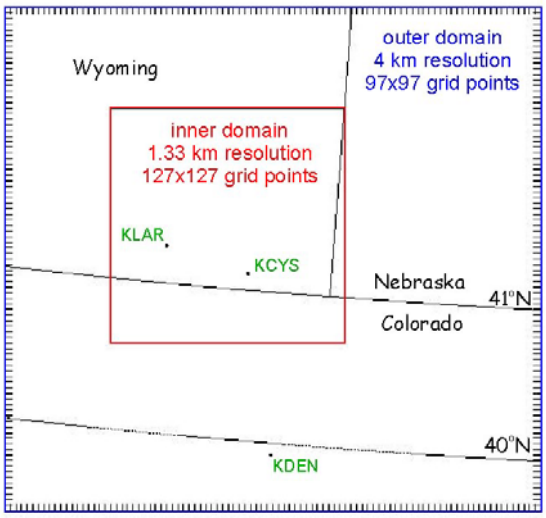

Figure 25: Outer and inner nest domain for the WRF simulations, with Laramie (KLAR), Denver (KDEN) and Cheyenne (KCYS) locations highlighted.

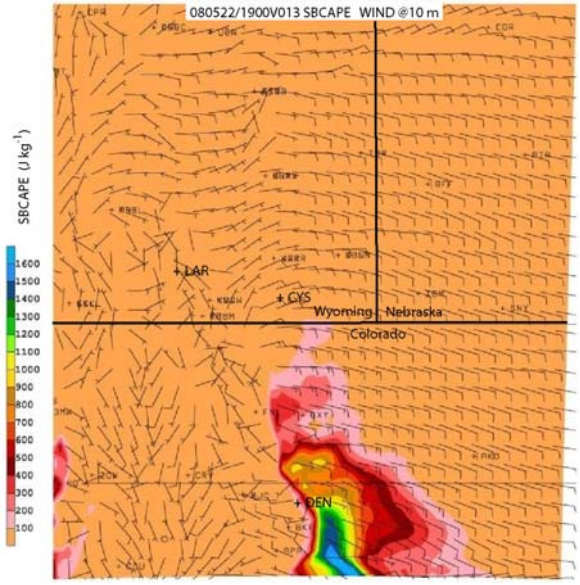

Figure 26: SBCAPE and 10 m winds at 1900 UTC in the outer WRF domain. Three-letter station identifiers are added to place model output in its geographic context. Click image to enlarge.

Long filaments of high cyclonic vorticity were produced both in the outer and inner WRF domains on the east side of the Front Range (Fig. 28). These "banners" were aligned with the steep Front Range and were best developed near Fort Collins, while remaining absent over the plains east of Cheyenne. They were aligned roughly with the 0-5 km shear vector, best defined between 700-500 hPa, and

present early in the day, clearly preceding convective development. The cyclonic banners alternated with

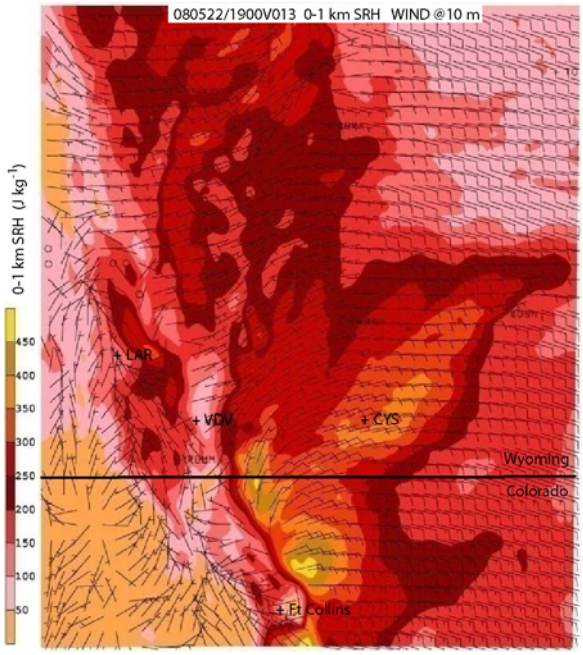

Figure 27: 0-1 km AGL SRH and 10 m winds at 1900 UTC in the inner WRF domain. Click image to enlarge.

much weaker anticyclonic banners (Fig. 28), consistent with the larger-scale cyclonic vorticity in the WRF-NMM (Fig. 24). The maximum cyclonic vorticity in these banners was between 10^{-3} and 10^{2} s^{1}, i.e., higher than in the WRF-NMM (because of the finer resolution in the WRF inner domain) and close to the observed vorticity of mesocyclone 'A'. In terms of potential vorticity (PV), the WRF outer and inner domains simulated multiple PV banners stretching from the Front Range into Wyoming, with a value as high as 40 PV units (PVU) between 700-600 hPa at 1800 UTC (about the time of convective initiation in this simulation), and 60 PVU at 1900 UTC, in a lens near Fort Collins (Fig. 28)[1].

WRF-simulated reflectivity from resolved convection between Laramie and Cheyenne at 2000 UTC exceeded 65 dBZ, as observed (Fig. 12). The WRF produced surface winds from the north-northeast at 1800 and 1900 UTC (Fig. 27), yielding 0-1.5 km SRH of ~400 m2 s-2 near Harriman, also consistent with observations (Fig. 22).

Potential vorticity is conserved and only can be generated by diabatic processes and friction. Several studies have simulated banners of high PV that form along the margin and in gaps of mountain ranges,

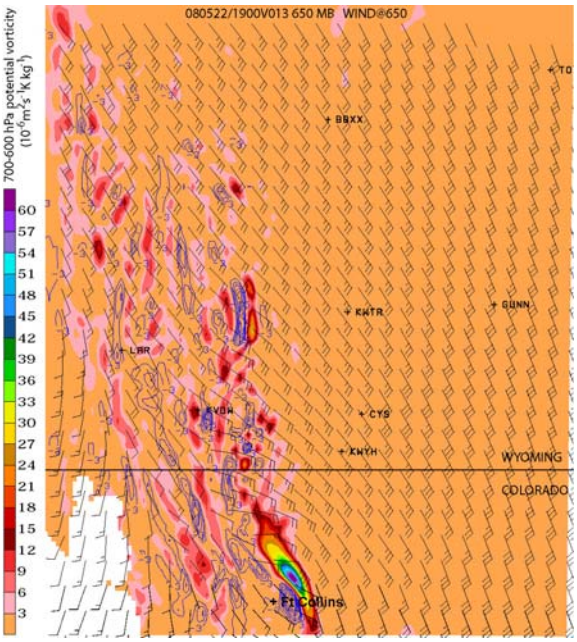

Figure 28: Potential vorticity between 700-600 hPa and 650 hPa wind (barbs) at 1900 UTC in the inner domain. Positive PV values are color-filled (in PVU) while negative vorticity is shown in blue contours (interval of 3 PVU). The white area in the lower left corner has terrain above 700 hPa. Click image to enlarge.

such as the Alps (e.g., Aebischer and Schär 1998; Schär et al. 2003; Grubišić 2004). Such banners tend to trail far downstream because of PV conservation. The PV banners in the WRF outer domain clearly formed along the Front Range, near the southern end of the domain and strengthened toward the north, suggesting that they were generated by friction along the eastern slopes of the Front Range. This corresponds well with simulations over the Alps (Aebischer and Schär 1998). In both cases, the strongest cyclonic PV banner was found on the right side of the steep terrain, looking downwind.

The reflectivity maximum of this cell was located just west of the vorticity maximum, corresponding with the PV maximum in Fig. 28. This cell traveled to the north, located by 2000 UTC over high terrain between Cheyenne and Laramie, again with a cyclonic vorticity maximum (about 5×10^{-3} s^{-1}) just to its east. The WRF convection was elongated along the deep-layer mean wind, as observed (Fig. 12), and patches of higher cyclonic vorticity tend to occur in or near the simulated convection. Thus the WRF simulation provides circumstantial evidence for the hypothesis that *mesocyclones can acquire some of*

[1]The conventional boundary between tropospheric and stratospheric air in mid-latitudes is merely 1-2 PVU.

their spin from the environment in which the convective storm grows. This hypothesis has been

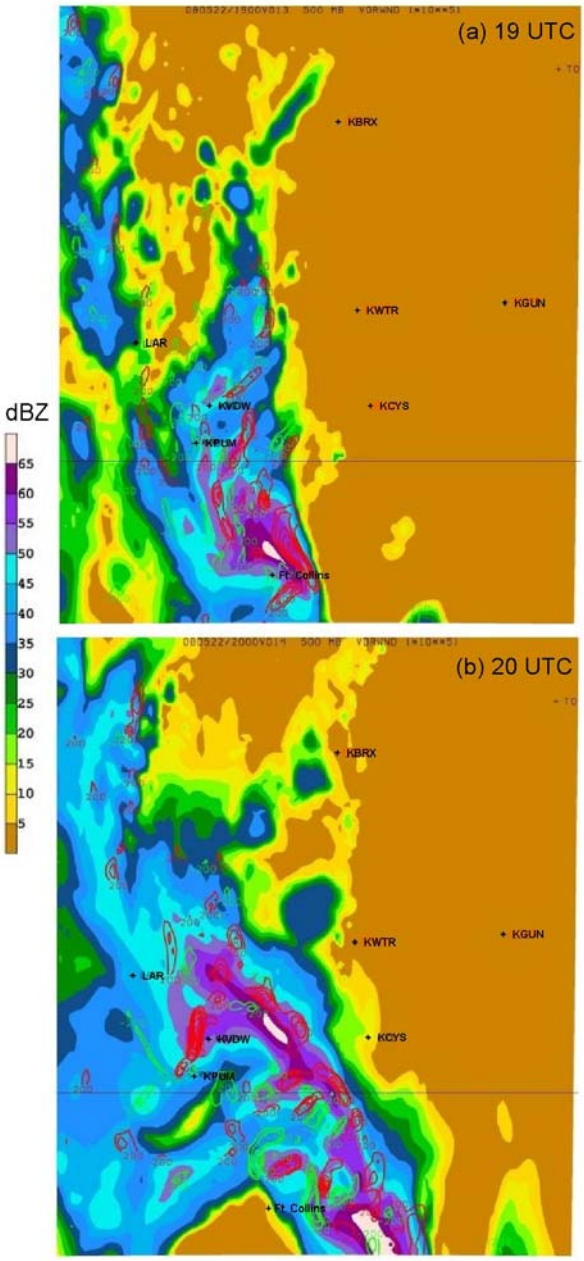

Figure 29: Maximum reflectivity at any level, calculated from the WRF bulk microphysics scheme assuming Rayleigh scattering (color fill, dBZ), overlaid with 500 hPa positive (red contours) and negative (green contours) relative vorticity (contour interval: 5×10^{-4} s^{-1}) in the inner domain, at (a) 1900 UTC and (b) 2000 UTC. Click image to enlarge.

confirmed along pre-existing shear lines (e.g.,Atkins et al. 1999) but to our knowledge, this is the first study that demonstrates that *orographically-induced* PV banners can be the source of ambient vertical vorticity. It should be noted that this process does not exclude mesocyclogenesis by the tilting of horizontal vorticity by a convective updraft in the presence of high SRH. In fact, the SRH of the inflow for storm 'A' was high (~200 m^2 s^{-2}) in the vicinity of Denver airport where storm 'A' first formed, and about twice as high near Harriman where it spawned its second tornado (Fig. 21).

The WRF simulation developed deep convection near the vorticity banners, and the convection breaks up the rather continuous streamers into smaller patches (Fig. 29). A vigorous, elongated convective cell can be seen in the inner domain near Fort Collins at 1900 UTC (Fig. 29a).

Finally, our modeling work does not show whether PV banners can affect the location of convective *initiation*. Our WRF simulations show that some storms in the outer and inner domains develop within a banner of high PV, while others grow in a low PV environment. The impact of orographically-induced PV anomalies on convective initiation and on mesocyclogenesis should be explored further.

7. Conclusions

Observations and numerical simulations are used to study an unusual tornadic mesocyclone on 22 May 2008 in southeastern Wyoming. The supercell first formed in the frontal warm sector about two hours before solar noon and spawned an EF3 tornado near Windsor, CO. It progressed as part of a mesoscale convective system over a quasistationary warm front, and produced a second tornado (the Laramie event) as it ascended about 1 km of gently sloping terrain. The latter mesocyclone formed and persisted in an environment with considerable low-level shear and SRH (~400 m^2 s^{-2}) but with little SBCAPE (500-750 J kg^{-1}) and no SBCIN. As the storm ascended the terrain, it intensified even though SBCAPE decreased along the track, while producing large hail, an intense mesocyclone with radar-estimated low-level shear as high as 84 m s^{-1} km^{-1}, a weak-echo region, and an EF2 tornado. This fast-moving mesocyclone entered an environment with virtually no SBCAPE, yet it could be tracked by the nearest Doppler radar for over 90 min, while only slowly weakening.

Near-surface Doppler radar observations, station data, and numerical simulations suggest that the formation and maintenance of the mesocyclone in this low-CAPE environment benefited from two terrain-related factors: 1) The observed channeling of low-level flow, locally enhancing SRH, and 2) As indicated by model output, banners of high PV generated by strong southerly flow shearing around the Colorado Front Range. The mesocyclone may

have acquired at least some of its vertical vorticity from a PV banner.

ACKNOWLEDGMENTS

This work greatly benefitted from discussions with Melissa Kreller and three reviewers. The SPC mesoscale analysis fields were provided by Jeffry Evans.

REFERENCES

Aebischer, U., and C. Schär, 1998: Low-level potential vorticity and cyclogenesis to the lee of the Alps. *J. Atmos. Sci*., **55**, 186-207.

Anderson, C. J., C. K. Wikle, Q. Zhou, and J. A. Royle, 2007: Population influences on tornado reports in the United States. *Wea. Forecasting*, **22**, 571–579.

Atkins, N. T., M. L. Weisman, and L. J. Wicker, 1999: The influence of preexisting boundaries on supercell evolution. *Mon. Wea. Rev.*, **127**, 2910–2927.

Boatman, J. F., and R. F. Reinking, 1984: Synoptic and mesoscale circulations and precipitation mechanisms in shallow upslope storms over the western High Plains. *Mon. Wea. Rev.*, **112**, 1725–1744.

Bosart, L. F., A. Seimon, K. D. LaPenta, and M. J. Dickinson, 2006: Supercell tornadogenesis over complex terrain: the Great Barrington, Massachusetts, tornado on 29 May 1995. *Wea. Forecasting*, **21**, 897–922.

Bothwell, P. D., J. A. Hart, and R. L. Thompson, 2002: An integrated three-dimensional objective analysis scheme in use at the Storm Prediction Center. Preprints, 21st Conf. on Severe Local Storms, San Antonio, TX, Amer. Meteor. Soc., J117–J120.

Braun, S. A., and J. P. Monteverdi, 1991: An analysis of a mesocyclone–induced tornado occurrence in Northern California. *Wea. Forecasting*, **6**, 13–31.

Brooks, H. E., C. A. Doswell III, and J. Cooper, 1994: On the environments of tornadic and nontornadic mesocyclones. *Wea. Forecasting*, **9**, 606–618.

____, ____, and M. P. Kay, 2003a: Climatological estimates of local daily tornado probability for the United States. *Wea. Forecasting*, **18**, 626–640.

____, ____, D. Dowell, R. Holle, R. Johns, D. Jorgenson, D. Schultz, D. Stensrud, S. Weiss, L. Wicker, and D. Zaras, 2003b: Severe thunderstorms and tornadoes. *Handbook of Weather, Climate, and Water*. T. D. Potter, and B. R. Colman, Eds., Wiley Interscience, 973 pp.

Brown, R. A., and V. T. Wood, 1991: On the interpretation of single-Doppler velocity patterns within severe thunderstorms. *Wea. Forecasting*, **6**, 32–48.

Doswell, C. A. III, and E. N. Rasmussen, 1994: The effect of neglecting the virtual temperature correction on CAPE calculations. *Wea. Forecasting,* **9**, 619-623.

Ek, M. B., K. E. Mitchell, Y. Lin, E. Rogers, P. Grunmann, V. Koren, G. Gayno, and J. D. Tarpley, 2003: Implementation of Noah land surface model advances in the National Centers for Environmental Prediction operational mesoscale Eta model, *J. Geophys. Res.*, **108** (D22), 8851, doi:10.1029/2002JD003296.

Elson, D., J. Wolfe, C. Dalton, and W. R. Schneider, 2008: Evolution of a wintertime Pacific Northwest mini-supercell and tornado. Preprints, *24th Conf. on Severe Local Storms*, Amer. Meteor. Soc., Savannah, GA, 13B.4. [Available online at http://ams.confex.com/ams/pdfpapers/141838.pdf]

Evans, J. S., and R. H. Johns, 1996: Significant tornadoes in the Big Horn Mountains of Wyoming. Preprints, *18th Conf. on Severe Local Storms*, San Francisco, CA, *Amer. Meteor. Soc.*, 636-640. [Available online at http://www.spc.noaa.gov/publications/evans/bighorns.htm.]

Finch, J. M., cited 2009: The Cheyenne Ridge tornado, April 23 1960. [Available online at http://bangladeshtornadoes.org/UScases/042360/042360tornado.html.]

_____, and D. Bikos, cited 2009: May 22 2008 tornado outbreak. [Available online at http://bangladeshtornadoes.org/UScases/052208/22may2008terrain.html.]

Fujita, T. T., 1989: The Teton-Yellowstone tornado of 21 July 1987. *Mon. Wea. Rev.*, **117**, 1913–1940.

Geerts, B., and Q. Miao, 2005: The use of millimeter Doppler radar echoes to estimate vertical air velocities in the fair-weather convective boundary layer. *J. Atmos. Oceanic Technol.*, **22**, 225–246.

Grubišić, V., 2004: Bora-driven potential vorticity banners over the Adriatic. *Quart. J. Roy. Meteor. Soc.,* **130,** 2571-2603.

Hart J. A., and W. Korotky, 1991: The SHARP workstation v1.50 users guide. National Weather Service, NOAA, U.S. Department of Commerce, 30 pp. [Available from NWS Eastern Region

Headquarters, 630 Johnson Ave., Bohemia, NY 11716.]

Homar, V., M. Gaya, R. Romero, C. Ramis, and S. Alonso, 2003: Tornadoes over complex terrain: an analysis of the 28th August 1999 tornadic event in Eastern Spain. *Atmos. Res*., **67-68**, 301-317.

Horel, J., and Coauthors, 2002: Mesowest: cooperative mesonets in the Western United States. *Bull. Amer. Meteor. Soc.*, **83**, 211-225.

Horgan, K. L., D. M. Schultz, R. H. Johns, J. E. Hales, and S. F. Corfidi, 2007: A five-year climatology of elevated severe convective storms in the United States east of the Rocky Mountains. *Wea. Forecasting*, **22**, 1031-1044.

Houze R. A., 1993: *Cloud Dynamics*. Academic Press, 573 pp.

Janjić, Z. I., 1996: The Mellor–Yamada level 2.5 turbulence closure scheme in the NCEP Eta Model. Research Activities in Atmospheric and Oceanic Modeling, WMO, Geneva, CAS/JSC WGNE, 4.14–4.15. [Available from World Meteorological Organization, Case Postale 2300, CH-1211 Geneva, Switzerland.].

Lin, Y. -L., R. D. Farley and H. D. Orville, 1983: Bulk parameterization of the snow field in a cloud model. *J. Appl. Meteor.*, **22**, 1065-1092.

Markowski, P. M., and J. M. Straka, 2000: Some observations of rotating updrafts in a low-buoyancy, highly sheared environment. *Mon. Wea. Rev.*, **128**, 449–461.

____, ____, E. N. Rasmussen, and D. O. Blanchard, 1998: Variability of storm-relative helicity during VORTEX. *Mon. Wea. Rev.*, **126**, 2959–2971.

Mitchell, E. D., S. V. Vasiloff, G. J. Stumpf, A. Witt, M. D. Eilts, J. T. Johnson, and K. W. Thomas, 1998: The National Severe Storms Laboratory tornado detection algorithm. *Wea. Forecasting*, **13**, 352–366.

Parker, W. P. and R. P. Hickey: 1980: The Cheyenne tornado of 16 July 1979. *Natl. Wea. Dig.*, **5**, 45-62.

Rasmussen, E. N., and D. O. Blanchard, 1998: A baseline climatology of sounding-derived supercell and tornado forecast parameters. *Wea. Forecasting*, **13**, 1148–1164.

Schär, C., M. Sprenger, D. Luethi, Q. Jiang, R. B. Smith, and R. Benoit, 2003: Structure and dynamics of an alpine potential vorticity banner. *Quart. J. Roy. Meteor. Soc.*, **129,** 825–855.

Skamarock, W. C., J. B. Klemp, J. Dudhia, D. O. Gill, D. M. Barker, M. D. Duda, X. Y. Huang, W. Wang, J. G. Powers, 2008. A description of the Advanced Research WRF Version 3. NCAR Tech. Note 475. [Available online at http://www.mmm.ucar.edu/wrf/users/docs/arw_v3.pdf.]

Thompson, R. L., and R. Edwards, 2000: An overview of environmental conditions and forecast implications of the 3 May 1999 tornado outbreak. *Wea. Forecasting*, **15**, 682-699.

____, C. M. Mead, and R. Edwards, 2007: Effective storm-relative helicity and bulk shear in supercell thunderstorm environments. *Wea. Forecasting*, **22**, 102–115.

Torres, S. M., and D. S. Zrnic, 2004: Range and velocity ambiguity mitigation techniques for the WSR-88D weather radar. Geoscience and Remote Sensing Symposium, IGARSS 2004. *Proc. IEEE*, **3**, 1727–1729, doi: 10.1109/IGARSS.2004.1370665.

Vasiloff, S. V., 1992: Comparison of several mesocyclone and tornado detection algorithms. OSF Rep., 50 pp. [Available from National Weather Service Radar Operations Center, 1200 Westheimer Dr., Norman, OK 73069].

Weisman, M. L., and J. B. Klemp, 1982: The dependence of numerically simulated convective storms on vertical wind shear and buoyancy. *Mon. Wea. Rev.*, **110**, 504–520.

____, and ____, 1984: The structure and classification of numerically simulated convective storms in directionally varying wind shears. *Mon. Wea. Rev.*, **112**, 2479-2498.

Wilson, J. W., T. M. Weckwerth, J. Vivekanandan, R. M. Wakimoto, and R. W. Russell, 1994: Boundary layer clear-air radar echoes: Origin of echoes and accuracy of derived winds. *J. Atmos. Oceanic Technol.*, **11**, 1184–1206.

Wolfe, J. P., J. R. Snider and B. Geerts, 2008: Development of a temperature-dependent radar reflectivity to snowrate relationship for the S-band. *Proc. 15th International Conf. on Clouds and Precipitation*, Cancun, Mexico, P13.14. [available online at http://cabernet.atmosfcu.unam.mx/ICCP-2008/abstracts/Program_on_line/Oral_13/WolfeEtAl_extended.pdf.]

Zeitler, J. W., and M. J. Bunkers, 2005: Operational forecasting of supercell motion: Review and case studies using multiple datasets. *Natl. Wea. Dig.*, **29**, 81–97.

REVIEWER COMMENTS

[Authors' responses in *blue italics.*]

REVIEWER A (Victor Homar):

Initial Review:

Recommendation: Accept with minor revisions

General Comments: This paper provides a very exhaustive and detailed analysis of the available observations of a tornadic mesocyclone [that] occurred on 22 May 2008 near the WY-CO border. The text is well written and the reader is exquisitely guided along the exposition of observations and results. The research is interesting as it discusses the formation and evolution of a special convective system that climbed up complex orography towards the northwest. The authors do a great job in discussing this particularities and connecting this case with typical academic examples. All statements are either well founded on observations or clearly presented as hypothesis, which helps following the long description of observations available for this case.

[Minor comments omitted...]

Second review:

General Comments: After revising the responses to the reviewers comments and reading again the paper, I believe the document is almost ready for publication as it has notably improved readability despite the addition of new material as suggested by other reviewers. Again, I believe the points are clearly made across and supported with adequate media.

A point I'm not comfortable with is the present version of the discussion of the PV banners. I realize one of the referees mentioned the lack of unequivocal proof of their role in the convective activity and further tornadogenesis. However, in my opinion the present version of section 6 uses too many speculative expressions. In particular, I think "at least" is used here without any clear reason for the new reader. It is clear it originates from one of the reviewer's comments but I think the text is not improved by adding this speculative component. These intense PV banners have definitely influenced the vertical velocity formation despite no unequivocal proof is provided (numerical experiments could help but are beyond the scope of this work). I think the paper benefits from describing the presence of these features but not so if they must be described under these too much (IMHO) speculative terms.

Upon reading Section 6 again, we agree that the speculative nature is a bit exaggerated, as a result of one of the reviewers' comments. The presence of PV banners is clear; they existed in the model before deep convection erupted. We have conducted some more numerical experiments, largely independent of this paper. It is clear in the animations that the modeled deep convection acquired at least some of its vertical vorticity from the PV banners. The text is more definitive, less speculative, except with regard to the relation between convective initiation and the PV banners. The term "at least" has been removed. In the interest of focus & paper length, we need to remain short about this topic, but we have enough model output on this that we may write another paper, specifically on PV banners & convective mesocyclones.

[Minor comments omitted...]

REVIEWER B (Peter C. Banacos):

Initial Review:

Reviewer recommendation: Accept with major revisions

Overview: This paper documents a long-lived, fast-moving supercell thunderstorm on 22 May 2008 that began near the Denver International Airport in its incipient stage, and tracked northwestward into southeastern Wyoming

producing one or more tornadoes from near the border community of Harriman, WY to the east side of Laramie, WY. This was the same supercell that produced the Windsor, Colorado tornado which received considerable national media attention. The case is made interesting by the fact that the Wyoming tornadoes occurred north of a quasi-stationary front.

While the premise of this paper fits well with the goals of the EJSSM and the overall writing style is excellent, there exist several significant flaws and unsubstantiated aspects in scientific reasoning that need to be addressed before publication. The scientific problems are outlined in the substantive comment section below. The presentation is also quite lengthy and unfocused at times, making it difficult for the reader to know what they should take away from the paper.

I think the authors could revise the manuscript to focus on why there was CAPE with surface temperatures only in the 40s Fahrenheit, a point that never comes across in the current version. That seems to be a more interesting place to start, rather than to downplay the 500 to 750 J/kg CAPE they acknowledge exists. In the current version, things like cloud-top temperatures from satellite seemed peripheral to what the paper is about, and makes it confusing for the reader to understand the key points being made.

In Section 4, I would think an organization structure that is chronological would be superior to individually focusing on one dataset at a time. Lastly, some of the figures were difficult to read (i.e., low resolution/fuzzy), and zooming in significantly didn't help much. My overall impression was that the paper is more a collection of parts at this point, rather than a focused, concise research paper.

Starting in the Introduction, and in the core of the paper as well as in the Conclusion, we emphasize the rather low surface temperature and high surface RH conditions of this high-elevation tornado. The high elevation and high RH yield a high equivalent potential temperature (θ_e), about 328 K, and that turns out to be essential. A saturated parcel at 8500 ft MSL, near the ground over SE Wyoming, with θ_e 328 K, has the same moist static energy (or CAPE-potential) as a parcel at sea level, with T=88°F and T_d=51°F.

A few figures have been resampled at higher resolution, for better zoom-in viewing. The structure of the paper has not been altered fundamentally (chronological sequence instead of the current sequence (i.e., synoptic-scale to finer scale maps, then vertical structure, then model output), although the revised version reads more fluently. The chronological sequence would be difficult given the diverse set of measurements and model output, including our own WRF simulations.

Substantive Comments:

1.) In the Introduction, the authors spend time discussing what is unusual about the environment associated with this particular tornado. In that discussion, they fail to mention that surface temperatures were only in the 40s Fahrenheit, and that the tornado occurred in "dense fog" per eyewitness reports near Imson Pond (elevation 7820 ft). These accounts are included on the Finch/Bikos website the authors' reference (i.e., http://bangladeshtornadoes.org/UScases/052208/22may2008terrain.html). I also feel that the authors spend too much time trying to argue that the environment had "low CAPE values". Given the cool surface conditions with fog, the thrust of the discussion should instead be on why there *was* CAPE at all! The combination of the high elevations and cold temperatures aloft actually allowed for theta-e decreasing with height (a potentially unstable environment). Isn't that what is truly important? Furthermore, the absence of CIN in the tornadic environment is not unusual. Many Southeastern U.S. tornado events feature low CAPE with minimal CIN, low LCL heights, and strong low-level SRH. In fact, it's hard to see why the presence of CIN would be favorable in any potentially tornadic environment, except perhaps to keep the convection somewhat more isolated, all else being equal.

We agree with most comments and have rewritten the Introduction accordingly. In particular, we emphasize the rather low surface temperature, low mixing ratio, yet high surface RH environment in which this high-elevation tornado occurred. We agree that a low CIN/high SRH environment is not unusual for tornadoes, and that significant CIN is not favorable in any potentially tornadic environment.

2.) Along the same lines as above, I would disagree that the Wyoming tornado was "continuously fed by warm-sector air", as stated on Page 7. If we can agree that at the time a parent thunderstorm is producing a tornado it is by default surface-based, then it must be the case that this storm had the cool east-northeasterly air north of the boundary as its inflow, not the warmer air south of the differential heating boundary in Colorado. Again, this is where the authors need to focus more attention on the fact that there was actually surface-based CAPE north of the boundary owing to the high elevations involved and cold temperatures aloft. I don't see evidence of the mixing arguments north of the boundary put forth by the authors in Section 4b. It would also be inconsistent to make the argument that the storm in question was "continuously fed by warm-sector air", and then later on Page 8 and in Fig.15 make the argument that PBL horizontal convective rolls between Laramie and Cheyenne were important to the tornadogenesis! The latter seems plausible to me, but much of Section 4b needs to be overhauled.

We removed the statement that the tornadic storm was continuously fed by warm-sector air. Certainly Storm A was fed entirely by warm-sector air early in its growth period (17-19 UTC, including the period of the F4 Windsor tornado). An analysis of the equivalent potential temperature (θ_e) (a new animation in the paper) field shows that θ_e does decrease to the north along the storm track, but that the decrease is small, at least up to the WY-CO state line. Also, the θ_e gradient across the warm front is remarkably small (notwithstanding the large temperature gradient), because of the dry air in the warm sector. Closer analysis suggests that the developing dryline intersected or moved over the warm front in eastern CO by 20 UTC. We agree with the reviewer that the Storm A's inflow near the WY-CO state line contained BL air originating from the cold side of the warm front. Note that the warm-frontal radar fine line (well-defined in eastern CO), becomes invisible towards Ft. Collins, suggesting that a virtual potential temperature (θ_v) difference is absent, possibly as a result of earlier convection. A sharp θ_v gradient is essential for a well-defined surface front.

3.) In the introduction, it's interesting that the authors don't make reference to the 23 April 1960 Cheyenne ridge tornado, which bares resemblance to the current case, and much more so than the others mentioned (similar tornado track and early in the season).

This event has been referred to. We were not aware of it.

4.) Page 6: The use of a storm-relative helicity from the surface to 1500 meters (e.g., Fig. 8) was an unusual choice, compared to the conventional surface to 1 km or surface to 3 km calculations. Without an explanation, the reader is left wondering why this particular choice was made.

The text now discusses the depth of integration of SRH, as follows: "Upper integration bounds of 3 km and 1 km are used more commonly (e.g. Markowski et al. 1998), although what matters to mesocyclone formation is the SRH within the effective storm inflow layer (Thompson et al. 2007). Soundings and wind profiles near the tornadic supercell suggest that the inflow layer was relatively shallow (see below). We used an upper bound of 1.5 km AGL because only this SRH field was available in the NCEP WRF-NMM and 12 km NAM products." We agree that the depths you mention (0-1 km and 0-3 km) are indeed generally used, both in the literature and on websites showing operational model output. The problem is that the NCEP 12 km NAM output fields include a field "0-1.5 km SRH", but not a 0-1 km nor a 0-3 km SRH. The 4 km NAM output fields only include a 0-0.5 km SRH and a 0-1.5 km SRH. So we decided to show 0-1.5 km SRH (Fig. 8 and Fig. 21). In order to compare apples to apples, we computed 0-1.5 km SRH from the modified Denver sounding (Fig. 22) and from our own 1.33 km WRF model output.

5.) The near-surface saturated and nearly dry adiabatic 12-km NAM sounding structure in Fig. 21 looks unrealistic. In a saturated upslope flow, shouldn't the low-level lapse rate be moist adiabatic? I don't think a most absolute unstable layer (MAUL) would occur in this environment. Also, the authors state that the "virtual temperature correction" has been applied in the CAPE calculation in Fig. 21. I'd recommend referencing the following paper for those unfamiliar with what the authors' are talking about:

Doswell, C.A. III, and E.N. Rasmussen, 1994: The effect of neglecting the virtual temperature correction on CAPE calculations. *Wea. Forecasting,* **9**, 619-623.

Perhaps it is the cool near-surface temperatures involved with this case, but when I look at the parcel trace provided on the Skew-T/Log-P diagrams in Fig. 21 and 22, I would have expected the trace to be shifted slightly to the right to account for the surface virtual temperature correction being applied. Admittedly, this is a relatively minor point with the sounding.

We agree that the near-surface saturated and nearly dry adiabatic sounding in Fig. 21 is unusual, simply because it is potentially unstable and saturated, i.e. the instability cannot be sustained. This profile is the model initial field (in this case, the 12-km NAM at 18 UTC). Apparently absolute instability is not removed in the NAM initialization process. Not surprisingly, the model did produce convective precip during 18-19 UTC. Is the sounding unrealistic? Maybe not, given the strong upslope flow, although it would be quite confined in time & space. The text has been clarified. The Doswell and Rasmussen (1994) reference has been added, thank you. And finally, we used a $_e$ trace based on the virtual T correction in Figs. 21 and 22, thus moving it slightly to the right. Note that the CAPE values listed were computed numerically from the sounding data, and that Figs. 21 and 22 merely graphically illustrate the area of positive energy (CAPE).

6.) I would question the authors assertion at the start of Section 3 that the "large-scale flow pattern was quite unusual". Certainly, slow-moving, deep layer cyclones moving across the southern Great Basin and the Four Corners Region are relatively common in the spring, as are upslope flow regimes into Front Range. Perhaps if this statement were (1), put in context and (2) referenced, it might be better.

We cannot find a good reference in the literature, but in our experience, deep cyclones with very little tilt (cut-off lows) are more common in the Four Corners region in spring than in any other season, and the resulting deep upslope flow, combined with the lower stability in spring, probably explains the fact that month of May is climatologically the wettest in SE Wyoming and NE Colorado. We added a somewhat relevant reference for this (Boatman and Reinking 1984), and we have rephrased the text to provide some context, as suggested.

7.) The authors use the term "banner" 13 times (mainly in Section 6) to describe the potential vorticity field. I'm not clear how a banner is defined exactly. More importantly, I'm not convinced that the 700-500mb PV was relevant to the dynamics of the supercell. Absent the PV discussion, the environment contained strong low-level SRH and sufficient CAPE for supercell thunderstorms. To me, the connection to the PV field seems tenuous and circumstantial in nature. I'm not questioning so much that these areas of PV existed, but what role do they play in mesocyclone dynamics? How would the 700-500mb PV be ingested into a thunderstorm with the inflow layer below that? I don't think the authors make a strong enough argument in this respect; one can't simple say that high values of PV were there, and were therefore relevant.

It is likely that the well-established mechanism of mesocyclone formation and maintenance, i.e. the tilting of horizontal vorticity by a convective updraft in the presence of high storm-relative helicity (horizontal vorticity aligned with storm-relative flow) near the surface, was important, simply because the SRH values were high (~200 m^2 s^{-2}) in the vicinity of Denver airport (where storm A first formed) and higher even (~400 m^2 s^{-2}) near the WY-CO state line (where the storm spawned its second tornado). The upper-air and surface data density is insufficient to capture PV patterns, so we have to resort to model output. Our strongest argument is that in our rather simple 1.33 km resolution WRF simulations several storms develop in "PV banners", the most intense one (computed radar reflectivity up to 65 dBZ, and cloud tops up to 12 km MSL) associated with a cyclone with a resolved relative vorticity of 10^{-2} s^{-1} and a resolved PV of 60 PV units. This does not prove that the resolved mesocyclone was generated by stretching out ambient vorticity within the PV banner. Nor does it prove that the PV banner was instrumental in storm formation in the first place (i.e., that storms preferentially form in PV banner was). We do not address the second question, but do state the first one as a hypothesis, and provide some evidence in support. The evidence is mainly from the 1.33 km WRF output; more detailed simulations are needed to examine mesocyclone formation.

The one element of observational evidence we have is that mesocyclone A moved with the deep-layer mean wind and not clearly to the right of it, as would be expected for supercells in such environment (clockwise turning wind profile). Also, it has been shown that low-level mesocyclones developing along a pre-existing shear line can acquire at least some of their spin from the environment (e.g., Atkins et al. 1999). Our case is similar, the only difference being that the pre-existing shear belt is orographically generated. Dr. Steve Koch at NOAA ESRL (pers. comm., June 2009) is leading an effort to study this case using experimental data assimilation and

high-resolution simulations. He plans to further explore the hypothesis that the mesocyclone was generated and/or maintained by stretching out ambient vorticity within the PV banner.

8.) On page 10, I was unsure what the authors meant by a "counter-jet". Some clarification of this would be helpful for the reader.

The counter-jet refers to a jet on the opposite side of the radar. Such jet would be present if the flow were horizontally uniform. The text is changed to "since an identical inbound jet to the NE of KCYS is absent."

9.) On page 14 (and in Fig. 23), I disagree that the "overall 0-6 km shear profile was rather straight". There is significant low-level turning of the hodograph in the modified 18z Denver profile, which is clearly important for low-level mesocyclone formation and tornado production. I don't think one can ignore this strong low-level curvature in discussing propagation of rotating convection. This discussion needs improvement.

We agree. The comment actually refers to the 12 km NAM wind profile (Fig. 23, now Fig. 22), which is rather straight. The modified hodograph shows much more curvature between 0-1.5 km, and we agree that this is essential, as discussed in our reply to the previous comment. The text has been clarified.

10.) I take some issue with the use of the word "Dynamics" in the paper's title. I believe the paper focuses mainly on the "environmental conditions" associated with the mesocyclone, and not necessarily on the dynamics of the mesocyclone itself.

The title has been changed to: "A case study of a long-lived tornadic mesocyclone in a low-CAPE complex-terrain environment."

11.) Page 3, column two: The operational NAM from NCEP is run four-times daily, so it wasn't immediately clear to me what 4-km NAM run model the authors are referring to in the first sentence of Section 2b. It's likely the non-hydrostatic WRF-NMM high-resolution window run, but some clarification is needed here. I believe WRF-NMM is a more appropriate way to reference what the authors used.

The text is clarified that this regards the operational NCEP WRF-NMM high-resolution (4 km) run for the western United States region. This simulation ran only at 6 UTC initial time on 22 May 2008; clearly the NCEP CONUS 12 km NAM runs 4 times daily.

[Minor comments omitted...]

Second review:

General Points:

1.) The quality (resolution, in particular) of the figures is much improved in this iteration of the paper and makes it much easier for the reader to interpret what is shown. Likewise, all references appear in the body of the text.

2.) The authors have addressed most of the questions presented in my first review and that is greatly appreciated. However, despite the revisions, the overall presentation still seems unnecessarily long and unfocused to me. Items such as anvil top temperatures (Page 6) are peripheral to the thrust of the paper, which should probably focus more narrowly on why this storm produced a tornado north of the warm front in the cool, saturated air mass (e.g., the boundary layer roll discussion is excellent). Anything in the paper that does not contribute to explaining the existence of the Wyoming tornado could serve as a basis for further editing. The authors have done a lot of good detailed analysis work. My point is simply that they haven't focused the discussion in a way that ties the analysis work concisely together for the reader. By discussing sequentially satellite imagery, surface observations, radar, and soundings, the paper still seems like a "collection of parts" rather than a cohesive whole. I mentioned this in my first review: a chronological sequence of events which interweaves the various datasets may have been more effective.

We agree with the gist of this comment, that the paper is more a collection of parts than a single coherent story. The research started out that way. The paper has been edited again to make it more coherent, more focused, and tangential topics such as IR anvil top temperatures and corresponding height have been removed. We see some merit to a chronological sequence, but decided early on to pursue a topical sequence, starting with the synoptic environment in which the storm formed, then a description of the storm itself, then the vertical structure of stability and shear, and finally the presence & possible impact of PV banners.

Secondly, the paper seems to have a bit of a "split-personality", alternating between various model and observational data sources. The authors change between local WRF, WRF-NMM, and 12-km NAM data, seemingly out of convenience for what they are attempting to show. At times I wondered if the paper was more about numerical modeling issues or an observationally based paper. I can accept publication in the present form based on the science, but in my opinion, the organization is still not where it *could* be.

We now state more clearly that we use the 4 km WRF-NMM and the 12 km NAM data at the same level as the observations, i.e. to depict the larger-scale state of the atmosphere. The surface and radar observations then depict the storm-scale evolution. At the end of the paper we introduce our own high-resolution WRF simulations to examine the question of storm development in an orographically-generated PV banner. The text now clarifies this up front, so the reader will be less likely to have the impression of a split-personality paper that jumps between observations & model output. We omitted mention of poor CAPE/SRH estimates from the earlier (06 UTC) initializations of the 4 km WRF-NMM and the 12 km NAM.

3.) I failed to mention this in my first review: why was Inverse Distance Weight (IDW) used in the analyses instead of a more standard Barnes analysis? While some analysis "bulls-eyes" are inevitable in complex terrain, the quality of the objective analyses (e.g., Fig 10) seem to suffer from this choice. For instance, in Fig. 10 note the uneven spacing of contours between Cheyenne and Chugwater. A proper two-pass Barnes scheme would probably have been better here and is generally superior to IDW for most meteorological applications (i.e., when data tends to be sparse and uneven).

The software used, ARCView, does not have a Barnes scheme unfortunately. It only has IDW, Kriging, Nearest Neighbor, and Spline. By the way, the IDW (a.k.a serpentine) method is widespread in use for meteorological applications – e.g. for Mesowest temperature and humidity analyses (John Horel, pers. comm.). Also, a serpentine tool is used for all RH and temperature analyses in NWS Interactive Forecast Preparation System (IFPS). Anyway, the point remains that the region of interest is sparsely and unevenly covered by data, and the coverage resolution coverage is coarse compared to the terrain. So we have some bulls-eyes to deal with. This is also why we plot potential temperature rather than temperature. No change.

[Minor comments omitted...]

REVIEWER C (Jeffry S. Evans):

Initial Review:

Recommendation: Accept with major revisions

General Overview: The case in question is quiet remarkable and is an interesting event for further study. However, this reviewer has two primary concerns which need to be addressed prior to acceptance for publication.

1) The paper leans too heavily on model data to provide support for the author's scientific claims regarding the case. Although the NAM and other high resolution models may be representative, the primary support should come from observational platforms that are available. For instance, why aren't the Medicine Bow and Platteville profilers shown or referenced? Not only could they be useful in describing the observed winds aloft, but should also be able to discern the depth of the frontal intrusion. In addition, the RUC-derived mesoscale parameters from the Storm Prediction Center would provide some additional support to the storm environment discussion.

The text now discusses the wind profile at Medicine Bow WY, in Section 4b. The Med Bow profiles are shown below, but not included in the paper, in the interest of paper length. There is some low-level veering early on (15-16 UTC), possibly associated with the warm or occluded front, but low-level directional shear decreases between 16-20 UTC as strong southeasterly flow extends to the surface. The small amount of veering evident between 16-20 UTC at around 3 km AGL may represent the warm frontal surface. A more in-depth interpretation needs to take into effect diurnal and orographic effects. None of the wind profilers at Platteville CO was operational on this day. The extra radiosonde from Denver at 18 UTC thus is very important. We also examined the VAD wind profiles from the Denver and Cheyenne 88D radars.

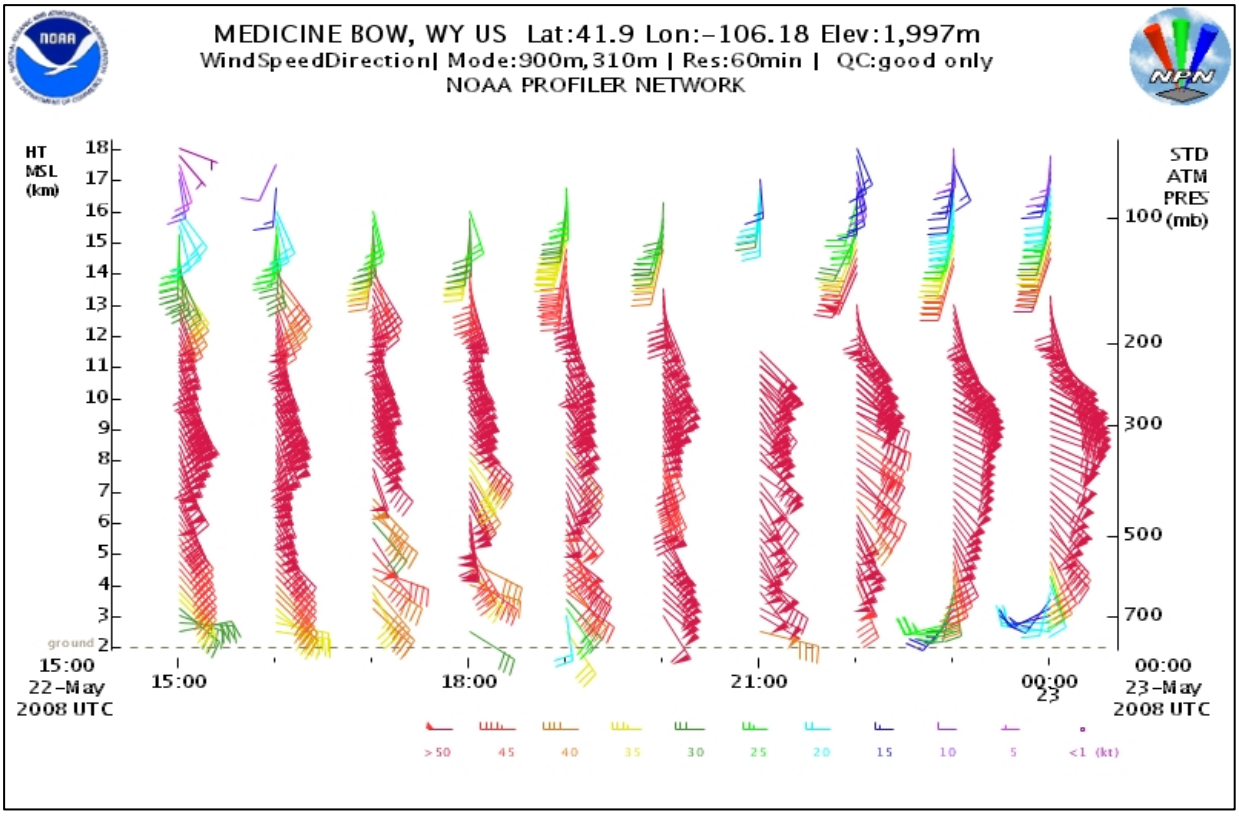

2) Why are the authors using the storm-relative wind data to describe the ambient winds over southeastern WY, in lieu of the base velocity data? The level 3 radar data uses a storm-average motion to derive the SRW fields, while the base velocity is unmodified and should be a better fit when they are discussing overall environmental winds.

We used both the Base Velocity and the Storm Relative Velocity data products. The former (in which the radial velocity field is ground-relative) was used to examine the channeling of the flow up the Laramie range and into the gap between the Laramie and Front Ranges. The latter is shown in Fig. 15 and Fig. 16 because the emphasis in this study is on the mesocyclone: the storm-relative velocity better reveals the mesocyclonic circulation. The text and figures (Fig. 15 and Fig. 16) have been clarified.

We have the received the regional mesoscale analysis maps from Jeffry Evans (Storm Prediction Center), and included one of them in the paper (Fig. 7b).

In addition, the figure captions tend to bleed into the text and make it hard to read. Please use slightly smaller font and try to keep the captions from bleeding into another column.

OK

1. Introduction
Should include a sentence on more recent work discussing the importance of greater values of low level theta-e/RH (I.e. LCLs) regarding maintenance of low level mesocyclones.

We are not sure what paper(s) the reviewer has in mind. We added one sentence, as follows: "In CAPE-starved environments storms with a low cloud base tend to be even weaker than those with a high cloud base (McCaul and Cohen 2002)."

3. Meso-alpha scale analysis
The discussion of low-level SRH does not appear relevant if storms north of the warm front are all based well above the surface. In which case, the low level winds are not ingested into the updrafts. Effective Helicity would be a more accurate field here.

A more careful analysis of the vertical structure and mapping of θ_e (included in the revised version) indicates that the θ_e gradient across the warm front is rather weak and that the inflow feeding storm A included the cooler air advected from the east, north of the warm front. Thus a discussion of low-level SRH is relevant. We now mention that effective SRH (Thompson et al. 2007) would be a more accurate field, but we do not have this field in the model output.

4. Meso-beta scale analysis
d. Radar Doppler velocity
Drop mention of the easterly low level winds being 'modulated' by the horizontal rolls unless you can prove this is occurring.

We believe we can prove this modulation. Ribbons of weaker outbound flow alternated with ribbons of stronger outbound flow over the Laramie Range, mainly between 1930-2000 UTC (Fig. 15). The orientation and wavelength of the velocity variations match that of the reflectivity variations (Fig. 12), thus the easterly flow was modulated by the roll convection.

5. Sounding analysis
b. Wind shear
In paragraph 3, you use low-level wind shear through 4 km, when the soundings suggest this is near the midpoint of the CAPE plot. Also, midway through this paragraph the authors contradict themselves by stating the SBCAPE/mixing ratios are unusually low for tornadoes, but then show these fields are not unusual via Fig. 24. Please reword.

We agree that it is more relevant to highlight the strong shear in the lowest km or so. The wind shear is 34 ms^{-1} over the lowest 1 km and 45 ms^{-1} in the lowest 4 km in the modified Denver sounding. The text has been changed. The contradiction you mention has been avoided by a rewording. The SBCAPE values are still rather low compared to most points in Fig. 24 (now Fig. 23, based on Brooks et al. (1994)).

[Minor comments omitted...]

Second review:

Recommendation: Accept with minor revisions

General Overview: The manuscript reads much better, although a few scientific and formatting issues remain which can be resolved easily.

1. Introduction
Drop 'weak' from sentence describing the SW flow at 500 mb with Big Horn Mountain tornadoes.

We did not omit it, but we changed it to "relatively weak" because the 500 mb flow in the case of the Big Horn Mountain tornadoes was 2-3 times weaker than the 2008/05/22 Laramie case. The limited data available in the

publications mentioned suggest that the 2008/05/22 Laramie mesocyclone may be the fastest-moving of all published Wyoming tornadic storms.

Did the tornadic storm form near a low-level baroclinic zone over southeastern WY, or was it the tornado? I think you meant the latter. Please reword.

You are correct. The storm 'A' clearly formed in the warm sector, but the Harriman-Laramie tornado was spawned after this storm moved north of the warm front. Text corrected.

Strike the discussions regarding cold-pool dynamics with the storm. The lack of much dry air below the cloud base would not be the only factor contributing to a strong cold pool. In addition, there has been an increasing amount of work in recent years discussing the importance of maintaining buoyancy (relatively higher levels of theta-e) within the RFD for tornadogenesis (See a few references below), instead of increased baroclinicity. Regardless, this discussion is not really needed here. The manuscript would read fine removing the sentences beginning, 'Thus, without a dry layer… ' and 'In CAPE-starved environments storms…'.

OK, we removed both sentences, but retained a short statement as follows: "Thus, without a dry layer below cloud base, convective cold-pool dynamics were likely of little significance in this case." This avoids the issue of BL baroclinicity and tornadogenesis.

Markowski P. M., J. M. Straka, and E. N. Rasmussen, 2002: Direct surface thermodynamic observations within the rear-flank downdrafts of nontornadic and tornadic supercells. *Mon. Wea. Rev*., **130**, 1692–1721.

Markowski P. M., 2002a: Hook echoes and rear flank downdrafts: A review. *Mon. Wea. Rev*., **130**, 852–876.

Markowski P. M., 2002b: Mobile mesonet observations on 3 May 1999. *Wea. Forecasting*, **17**, 430–444.

Grzych, M.L., B.D. Lee, and C.A. Finley, 2007: Thermodynamic Analysis of Supercell Rear-Flank Downdrafts from Project ANSWERS. *Mon. Wea. Rev*., **135**, 240–246.

[Minor comments omitted...]